Scratching the Surface: Fundamental Investigations of Tribology with Atomic Force Microscopy

Robert W. Carpick

Materials Sciences Division, Lawrence Berkeley National Laboratory, and Department of Physics, University of California at Berkeley, Berkeley, California 94720

Miquel Salmeron*

Materials Sciences Division, Lawrence Berkeley National Laboratory, Berkeley, California 94720

Received October 3, 1996 (Revised Manuscript Received March 31, 1997)

Contents

* Author to whom correspondence should be sent. Phone: (510) 486-6230. Fax: (510) 486-4995. E-mail: salmeron@stm.lbl.gov.

I. Introduction

A few years after the invention of the scanning tunneling microscope (STM), the atomic force microscope (AFM) was developed.[1] Instead of measuring tunneling current, a new physical quantity could be investigated with atomic-scale resolution: the *force* between a small tip and a chosen sample surface. Sample conductivity was no longer a requirement, and so whole new classes of important materials, namely insulators and large band-gap semiconductors, were brought into the realm of atomic-scale scanning probe measurements. The initial operation mode measured the vertical topography of a surface by maintaining a constant repulsive contact force between tip and sample during scanning, akin to a simple record stylus. However, since its inception, a myriad of new operation modes have been developed which can measure, often simultaneously, various sample (and even tip) properties. Perhaps the most notable extension so far of AFM capabilities was the realization that lateral forces between the tip and sample could also be measured.[2] It was thus recognized that the atomic-scale origins of friction could be probed with this technique, usually described as friction force microscopy (FFM). This, along with other types of AFM measurements, has established the AFM as an important tool in the emerging field of *nanotribology;* the study of the atomic-scale ingredients of interactions between surfaces in relative motion, such as friction, adhesion, lubrication, and wear.[3−8] This paper reviews progress and recent results obtained with AFM and other closely related techniques in the field of nanotribology, and attempts to point out many of the unresolved questions that remain.

The corresponding study of friction, adhesion, and so forth from a macroscopic and practical perspective is known, of course, as *tribology* and while this term was coined in the 1960s, these ideas have been pursued for centuries.[9] Most of this work has been performed in the domain of engineering because of the obvious practical importance: reducing energetic losses due to friction (*e.g.*, helping a car engine to work efficiently), utilizing friction as an operation mechanism (*e.g.*, car brakes), reducing material losses due to wear (*e.g.*, longer-lasting tires), and optimizing lubricants (*e.g.*, increasing the efficiency and lifetime of engine parts) are important issues for a wide range

S0009-2665(96)00068-4 CCC: $28.00

Robert W. Carpick is a Ph.D. candidate in the Department of Physics, University of California at Berkeley. He received his B.Sc. in Physics from the University of Toronto in 1991 and was awarded a 1967 Science & Engineering Scholarship from the Natural Sciences and Engineering Research Council of Canada for graduate work. His doctoral research in the group of Dr. Salmeron at Lawrence Berkeley National Laboratory has focused on atomic-scale tribology using ultrahigh vacuum atomic force microscopy and surface science techniques. He has probed relations between atomic-scale friction in the elastic regime and continuum contact mechanics. He was the recipient of the 1995 Russell & Sigurd Varian Fellowship from the American Vacuum Society in recognition of his thesis work and has been awarded a Postdoctoral Fellowship from the Natural Sciences and Engineering Research Council of Canada.

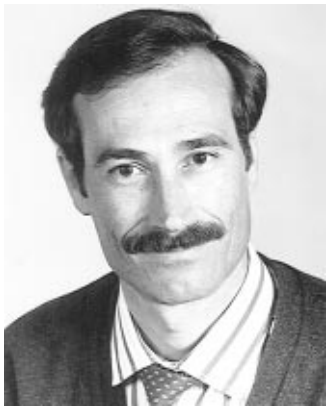

Miquel Salmeron is a Senior Staff Scientist and Principal Investigator in the Materials Sciences Division of the Lawrence Berkeley National Laboratory. He graduated from the University of Barcelona in 1967. He obtained a Master's Degree in solid-state physics from the Université Paul Sabatier, Toulouse, France, in 1970, and a Ph.D. in physics at the Universidad Autonoma de Madrid, Spain, in 1975. After spending two years as a postdoctoral fellow in Berkeley studying reactive scattering of molecular beams of hydrogen molecules on platinum, he returned to Spain in 1977. There he was an investigator in the Spanish Research Council (CSIC) and Professor of Physics at the Universidad Autonoma de Madrid. In 1984 he assumed his current position where he has since developed STM and AFM techniques and applied them to studies of surface structure, chemisorption, semiconductors and tribology. He has been recently elected to fellowship in the American Physical Society and received the awards for Sustained Outstanding Research in 1996 and for Outstanding Scientific Accomplishment in 1995 in the Materials Chemistry Category as part of the U.S. Department of Energy Materials Sciences Research Competition. He serves on the Editorial Advisory Board of *Tribology Letters*. He has taught at the University of Barcelona in Spain, at the Universidad Autonoma de Madrid in Spain, and at the University of California at Berkeley.

of industrial and indeed, societal applications. In fact, it is estimated that a substantial portion of the nation's gross domestic product is dispensed on energetic or mechanical losses due to friction and wear,[10] and a significant portion of this could realistically be recovered by improvements achieved through research.[11] With the advent of small devices triggered in part by the tremendous development of silicon microfabrication techniques,[12] novel problems appear that require knowledge at the nanometer scale. For example, the whole technology of information storage as exemplified by the case of computer hard disks with coatings and lubricants that protect the stored information, with dimensions that are measured in nanometers.[13] Micrometer-sized actuators, sensors, and motors are another example of novel technology requiring such knowledge for performance optimization.[14]

Despite the heavy volume of work performed so far,[6,8,11,15−17] there does not exist a fundamental understanding of tribological processes (although a great deal of practical successes have occurred). It would be fair to say that friction itself is one of the most common, yet least understood, physical phenomena. The main reason for this lack of understanding is that probing the atomic processes taking place at a buried interface is an inherently difficult task. The main conclusion of the earlier observations, as most high school physics students learn, is that friction between a pair of surfaces is proportional to load (normal force). Furthermore, friction is evidently independent of the apparent area of contact and only weakly dependent on the relative sliding velocity. This linear or nearly linear dependence of friction upon load is a result of complex phenomena at the interface, particularly multiple asperity contact,[18,19] adhesion-induced deformation,[15] and plowing of the surfaces by wear particles during sliding.[20] While these observations are important, they fail to explain the behavior at the atomic scale and cannot be used for predictive analysis.

At the fundamental level, friction, adhesion, and wear need to be understood in terms of chemical bonding and of the elementary processes that are involved in the excitation and dissipation of energy modes. Several mechanisms have been proposed that we shall enumerate briefly here and discuss in more detail later, in relation to specific examples discussed throughout this review. One is due to coupling to the substrate (and tip) electron density that causes a drag force, similar to that causing an increase of electrical resistance by the presence of surfaces in thin films.[21−25] Another is the excitation of surface phonon modes in atomic stick−slip events that will be discussed below. Delocalization of the excited phonons by coupling to other phonon modes through anharmonic effects and transport of the energy away from the excited volume leads to efficient energy dissipation.[26] At high applied forces, wear processes leading to rupture of many atomic bonds, displacement and creation of dislocations and debris particles, are important and are part of the wide topic of plastic deformation of materials. As we shall see later, another wear mechanism might be playing an important role in energy dissipation, where the extent of the damage is restricted to the creation of point defects near the surface by rupture of bonds due to the applied forces. Damage at this level is easily overlooked since as we discuss further below, true atomic resolution is not usually achieved in contact mode AFM.

The next level of complexity in our understanding include questions such as the nature of the relative motion between the two contacting bodies: is it continuous (smooth sliding) or discontinuous (stick−slip)? How does friction depend upon the actual area of contact between a pair of materials? Are friction and adhesion related? What is the behavior of lubricant molecules at an interface? How are they compressed and displaced during loading and shear? How does their behavior depend upon their molecular structure and chemical identity?

The relatively recent development of techniques that probe the properties of interfaces with either atomic-scale spatial or temporal resolution has generated great interest because these fundamental questions are beginning to be addressed. This excitement stems not only from the development of the AFM, but also from recent advances with other instruments to be briefly discussed below, namely, the quartz-crystal microbalance (QCM)[27−29] and the extension of the surface forces apparatus (SFA)[30,31] to measure frictional forces.[32,33] Furthermore, advances in computational power and theoretical techniques are now making sophisticated atomistic models and simulations feasible.[34]

By using these techniques to address the questions outlined above, the knowledge gained could be used in combination with the highly developed fields of chemical engineering, materials processing/synthesis, and engineering design to produce machines and devices with optimal tribological performance. However, this panacea is far from being realized. Not only does the atomic-scale knowledge remain to be discovered, but then the gap between this atomic-scale understanding and macroscopic application will need to be bridged. This is no small task and is beyond the scope of this paper. However, we will return to this issue in our concluding discussion.

The goal of this paper is to demonstrate that AFM is capable of producing this atomic-scale knowledge. As such, we will focus upon some of the contributions of the AFM to nanotribology. We will almost exclusively discuss results that shed light on the actual atomic and molecular processes taking place, as opposed to the more applied investigations of microscale properties which are also carried out with AFM. We will accompany this discussion by mentioning related theoretical efforts and simulations,[34] although our main emphasis will be upon experimental results and the techniques used to obtain them, as well as suggested future directions. In many ways, AFM techniques for quantitative, fundamental nanotribology are only in a nascent stage; certain key issues such as force calibration, tip characterization, and the effects of the experimental environment, are not fully resolved or standardized. We thus begin with a critical discussion of the relevant technical aspects with using AFM for nanotribology. We begin our discussion of nanotribology by presenting one example each of SFA and QCM results. We then discuss a wide array of results obtained with AFM. As this field is still in its infancy, results so far are generally sporadic in scope and direction; only a few systematic studies have been carried out, which we shall emphasize. For convenience, the AFM results will be grouped in two parts: first, studies of "bare interfaces" where the only materials involved are a contacting pair of surfaces, with some discussion of the effects of the experimental environment (humidity, contamination, *etc.*) and second, studies of "model lubricant films" where by design there exists at least one molecular layer of a material between a pair of surfaces. The first set of studies is generally aimed at gaining an atomic-scale understanding of processes such as interfacial (wearless) friction, the onset of wear, nanometer-scale elasticity and plasticity, and the role of adhesion. The second set of studies is generally aimed at gaining a fundamental understanding of how these processes are affected by interfacial layers, *i.e.*, lubricants.

II. Technical Aspects

A. Force Sensing

In an AFM experiment, a small sharp tip (with a radius typically between 10−100 nm) is attached to the end of a compliant cantilever (see Figure 1a). The tip is brought into close proximity with a sample surface in a fashion that is identical to STM tip−sample approach mechanisms. Forces acting between the AFM tip and the sample will result in deflections of the cantilever (Figure 1b). The cantilever bends vertically (*i.e.*, toward or away from the sample) in response to attractive and/or repulsive forces acting on the tip. When the tip is in contact with a sample, the deflection of the cantilever from its equilibrium position is proportional to the normal load applied to the tip by the cantilever. Lateral forces result in a twisting of the cantilever from its equilibrium position. These measurements can be performed in a variety of environments: ambient air, controlled atmosphere, liquids,[35] or ultrahigh vacuum (UHV).[36−39] AFM is certainly the most versatile tool for nanotribology in terms of operating environment.

Microfabricated cantilevers made of silicon and silicon nitride are commercially available. They are fabricated with a variety of force constants (anywhere from 0.01 to 100 N/m), high resonance frequencies, and very small yet reasonably durable integrated tips.[40−43] Other cantilevers, such as wires with chemically etched tips,[2] parallel leaf-spring assemblies with diamond tips,[44] and tips held by double cross-hair force sensors[45] are also in use and allow further choice of tip materials. To measure both normal and lateral deflections simultaneously, the optical beam deflection method[36,46,47] has proven to be the simplest to implement and is currently in use by all commercially available instruments and several custom designs.[48,49] In this scheme, a laser beam is reflected from the back of the cantilever into a position-sensitive quadrant photodetector. The method in fact measures the angles by which the cantilever is bent by applied forces, which for small angles is linearly proportional to the tip deflections. While relatively easy to use, its implementation is difficult in certain applications. In particular, for UHV or controlled environment experiments, external adjustment of the optical alignment is difficult but often necessary because the cantilever position may drift substantially with changes in temperature, pressure, and humidity.[50] This has been addressed

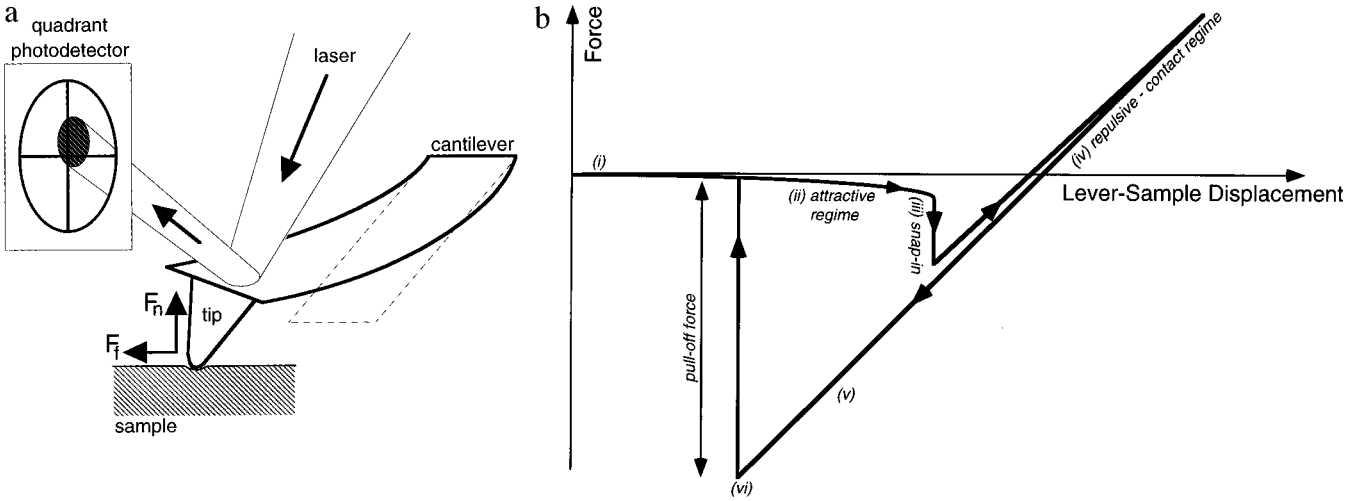

Figure 1. (a) Diagram of the AFM setup for the optical beam deflection method. The tip is in contact with a sample surface. A laser beam is focused on the back of the cantilever and reflects into a four-quadrant photodetector. Normal forces deflect the cantilever up or down, lateral forces twist the cantilever left and right. These deflections are simultaneously and independently measured by monitoring the deflection of the reflected laser beam. (b) An "approach curve" or "force−distance" curve displays the vertical cantilever bending *vs* lever−sample displacement. This displacement is measured between the sample and the rigidly held rear end of the cantilever (as opposed to the front end with the tip which will bend in response to interaction forces). (i) The lever and sample are initially far apart and no forces act. (ii) As the lever is brought close to the sample, the tip senses attractive forces which cause the end of the lever to bend downward, thus signifying a negative (attractive) force. (iii) The attractive force gradient exceeds the spring constant of the lever at this point, and this instability causes the tip to snap into contact with the sample. (iv) The lever−sample displacement can continue to be reduced. Since this tip is in repulsive contact with the sample, the front end of the lever is pushed further and further upward. The force corresponds to the externally applied load. (v) The motion is reversed. Adhesion between the tip and sample maintains the contact although there is now a negative (tensile) load. (vi) Finally the tensile load overcomes the adhesion or pull-off force and the tip snaps out of contact with the sample.

in various ways by different designs.[38,49] Another important consideration is that a force (*i.e.*, friction) acting on the tip *parallel* to the long axis of the cantilever will cause longitudinal buckling which is indistinguishable from that due to a normal force. This is particularly important when studying atomic-scale stick−slip behavior[51] and will be discussed further in section IV.A.1. Also, interference between the reflected beam and light scattered from the sample surface (due to imperfect focusing) can cause a measurable fluctuation in the signal and may lead to misleading results if not checked.[52]

Interferometry with a fiber optic[53−55] can also be utilized and in fact possesses higher sensitivity than optical beam deflection. The original interferometric FFM design[56] required precisely positioned individual fiber optics for normal and lateral force detection. Atomic-scale stick−slip motion was first detected with this design.[2] Recently, a modulation technique using a single fiber optic interferometer was shown to be capable of measuring normal and friction-induced longitudinal cantilever deflections (buckling)[57] using a microfabricated cantilever. However this method has not yet been shown to be sensitive to atomic-scale variations of the friction force. Piezoresistive cantilevers that can measure both lateral and normal deflections of the cantilever have recently been demonstrated.[58] Normal force resolution is currently below that of the optical deflection method due to the predominance of the Johnson noise of the resistive elements. Also, the authors do not quote a value for lateral force sensitivity, but improvements beyond this initial result are expected. Piezoresistive cantilevers are attractive for vacuum and other controlled-environment experiments, since complications due to optical elements are eliminated. Recently, high quality factor quartz oscillators with tips attached have been used as probes.[59−61] Tip−sample forces can be sensitively measured due to damping of the oscillator by the interaction forces.

It is important to realize that lateral forces arise not only from friction but also from the local surface slope, as discussed by several authors.[62−64] If the sample surface is not flat, the surface normal force will have a component directed laterally and will result in contrast in the lateral force image. This complication must be taken into account when analyzing FFM measurements and should be avoided by using flat samples whenever possible.

B. Force Calibration

While many striking *qualitative* properties are revealed in topographic and friction data (as many examples below will show), developing a fundamental understanding of these phenomena requires a *quantitative* analysis. Thus, whatever type of cantilever or detection method is employed, the measured signals must be accurately calibrated to yield forces. This requires, among other things, knowing the normal and lateral force constants of the cantilevers. Unfortunately this is a rather complicated task and no standardized method has yet emerged.

One way to estimate the force constants is to use formulae or calculations based on numerical methods. Formulae for the force constants of simple beam geometries are known[65] and can be applied for the case of wire cantilevers, or simple rectangular-shaped microfabricated levers. Many of the commercial microfabricated levers come in a "V" shape, the force

constants of which are complicated to calculate. Different formulae have been worked out by several groups[66−69] and have been compared to calculations based upon finite element analysis.[68,69] Only the work of Neumeister and Ducker[68] includes a formula for the lateral force constant. Their formulae are somewhat more complicated than the other references, but compare favorably with their own finite element analysis. Sader's formula for the normal force constant[69] has a simpler form, which also compares favorably to finite element analysis. Ogletree *et al.*[62] calculated normal and lateral force constants for certain commercially available V-shaped cantilevers. The calculations took into account more details of the shape of the cantilever which can have a significant effect in some cases.

For any of these calculations, all the cantilever dimensions and the relevant moduli of elasticity (Young's modulus, shear modulus, Poisson's ratio) are needed to calculate the force constants. The density is also needed to calculate the resonance frequency, which is a useful comparison because the free resonance frequency of these cantilevers is typically very easy to measure from the power spectrum of the cantilever's thermal vibrations. Such a measurement reduces the number of unknowns in the calculations.[70] In any event, the dimensions of the cantilevers are not easy to measure (a good scanning electron microscope is required, particularly to measure the submicrometer thickness of the cantilever which is a critical parameter), and the elastic moduli and density of the cantilever materials are uncertain. This is particularly true for silicon nitride levers as they are produced by chemical vapor deposition resulting in an amorphous structure with uncertain stoichiometry and residual stress. Furthermore, the cantilevers typically have a metal coating (usually gold) to enhance laser reflectivity, which affects the mechanical properties.[71] Finally, for the optical beam method, the position of the laser spot on the cantilever affects the calibration factors. Unfortunately this dependence is quite important and varies when optical realignment takes place.[62,72]

While these formulae and calculations are useful to obtain estimates of the forces applied, clearly from the above discussion it is much more desirable to have an *in situ* method of directly measuring cantilever force constants. Unfortunately, since the microfabricated levers are so small, nondestructive *in situ* testing is difficult. Nonetheless, some methods have been successfully implemented. These include measuring deflections or resonance frequency shifts for levers loaded with known masses,[73−75] and measuring the deflection of the cantilever when in contact with another lever of known spring constant.[76,77] Comparison of the cantilever's thermal noise with formulae can provide a calibration[78] although measurements of the cantilever's properties are still required. It is incorrect to use formulae which regard the cantilever as a point mass on the end of a massless spring, as was done in one paper.[79] Recently Ogletree *et al.*[62] have presented the only method so far which allows the lateral force sensitivity to be determined *in situ*. Currently, most AFM work has estimated forces from calculations like those mentioned above.[70] Further efforts may lead to more generally accepted practices for *in situ* force calibration. This effort is necessary to lead to reproducible and accurate quantitative results.

Proper signal and spatial calibration also requires knowing the sensitivity of the piezoelectric scanning elements. This can involve complications due to instrumental drift[80] and inherent piezoelectric effects, namely nonlinearity, hysteresis, creep, and variations of sensitivity with applied voltage.[81,82] Caution must be exercised when determining and relying upon these parameters. Techniques such as laser interferometry,[52] scanning sloped samples,[62,82] and scanning known surface step heights[83] or the use of precalibrated piezoelectrics[84] can facilitate piezo calibration.

In general, discussion or even statements of uncertainties in AFM measurements is often neglected. This important scientific aspect should not be ignored. A good introduction to aspects of error analysis with force microscopy is contained in the paper of Schwarz *et al.*[72]

C. Probe Tip Characterization

A problem of quite a different nature is that the geometry of the contact formed between the AFM tip and sample surface is not defined if the tip shape is not known. Furthermore the exact chemical composition of the tip is not easy to determine. Most results have not taken this into account or have made assumptions about the tip shape, presumably because of the inherent difficulty of directly measuring it. Yet this issue is of crucial importance: one is trying to understand the properties of an *interface*, and the tip is half of that interface. Its structure and chemical nature should thus be determined. Unfortunately, this difficulty is often not addressed in the literature. In fact, we will discuss an example below where different tip shapes and different tip materials indeed make a substantial difference in the results.[85]

Several *in situ* methods to characterize the tip shape have been discussed in the literature. A topographic AFM image is actually a convolution of the tip and sample geometry. Separation of the tip and sample contributions by contact imaging sharp or at least known sample features allows, *in situ*, some determination of the overall tip shape on a namometer to micrometer scale.[85−94] *Ex situ* tip imaging by transmission electron microscopy has also been performed.[93,95] Some of these measurements have revealed that a *majority* of microfabricated cantilevers possess double tips and other unsuitable tip structures.[88,94] This convincingly proves that tip characterization is absolutely necessary for useful nanotribological measurements with AFM. Thin film coatings applied to the microfabricated levers can provide robust, smooth, and possibly conductive coatings.[95−97] Further work in this direction would be useful, so as to provide a wider array of dependable tip structures and materials.

D. AFM Operation Modes

There are different force regimes in which forces can be measured with AFM. Figure 1b describes in

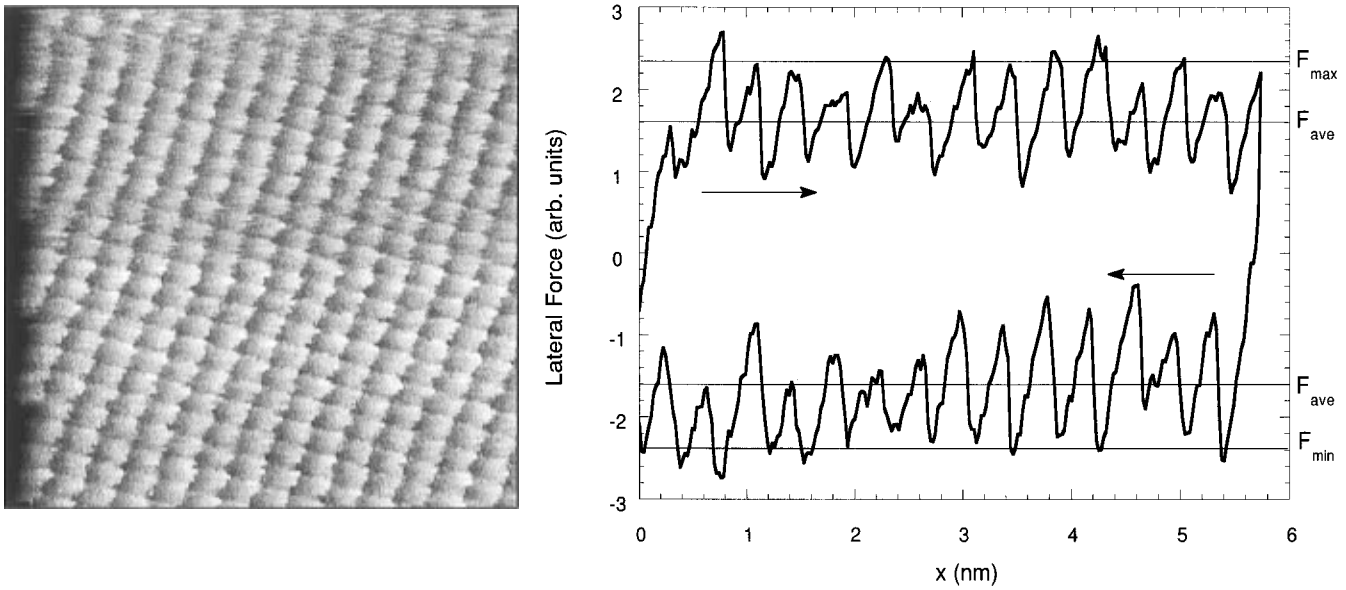

Figure 2. (a, left) A 6 by 6 nm^2 lateral force image of KF(001) cleaved and imaged in UHV with a silicon nitride tip. Stick−slip motion with the periodicity of the KF unit cell is observed. The scan direction is from left to right. (b, right) A "friction loop" from a single line of the image shown in a and the corresponding right to left lateral force image. The arrows indicate the scan direction for each half of the friction loop. The stick−slip motion is clearly evident. Hysteresis in the loop signifies that energy is dissipated. The average and maximum lateral forces for each scan direction are indicated. Data obtained by the authors.[101]

detail the normal force typically experienced by the tip as it is brought toward a sample surface. Two force regimes can be distinguished: the "attractive regime", where interaction forces (van der Waals, electrostatic, *etc.*) attract the tip to the sample but actual mechanical contact does not occur, and then the "repulsive" or "contact regime", where the outer electronic configuration of tip and sample atoms provide electrostatic and Pauli repulsive forces. On approach, these two regimes are separated by a snap-in instability which occurs when the attractive force gradient exceeds the spring constant of the cantilever. Further below we discuss how this instability can be prevented by applying forces directly to the tip. Interfacial surface forces between the tip and sample lead to adhesion during contact.

1. Normal Force Measurements

Initially AFM was applied to measurements of the topography of surfaces. As with STM, a feedback circuit is enabled to vary the relative vertical displacement as the tip is rastered across the sample. In this case the control signal kept constant is cantilever deflection instead of tunneling current. Such constant force images can be obtained in either the attractive or repulsive regimes. Several other methods such as ac modulation techniques can be used to image in the attractive regime, including the new "force modulation" technique[98] which has been demonstrated to achieve true atomic resolution on surfaces, but these techniques will not be discussed here as they are not directly employed for tribological applications.

It must be pointed out that when the tip is in mechanical contact with a given sample, simple elastic contact mechanics shows that for typical tip radii, loads and elastic constants, the contact is not just a single atom. For example, a 20 nm radius silicon nitride tip (sharp by AFM standards) exerting a 1 nN load (relatively low by AFM standards) on a mica sample produces a contact area involving nearly 15 mica unit cells, as estimated using the Hertz theory which in fact neglects adhesion. Including adhesion makes the contact area even larger and can ensure a substantial contact area even at the lowest possible applied loads. (See section IV.A.2 for more details.) Contact-mode AFM therefore does not possess single-atom resolution as with STM, and so point defects are not imaged, and the nature of observed atomic corrugations is complicated. This finite contact area is the essential limit on the lateral resolution of features and results in effects such as finite atomic step widths.

2. Lateral Force Measurements

The lateral twisting of the cantilever can be measured simultaneously with topography and often features that are not necessarily topographically distinct can show contrast in the lateral force signal due to different friction characteristics.[99,100] This suggests that friction imaging can have some degree of material or chemical sensitivity and will be discussed further below. Lateral force images often display atomic-scale stick−slip behavior with the periodicity of the atomic lattice of the sample. An example of a silicon nitride tip sliding on the KF-(001) surface in UHV is shown in Figure 2.[101] Atomic-scale stick−slip will be discussed in detail in section IV.A.1.

The *load dependence* of friction is an important measurement. (Examples will be given in section IV.A.2.) Typically, the average value of the frictional force while sliding at a given applied load is measured. This is done by taking half of the difference between the average lateral force measured while sliding in each scanning direction, a so-called "friction loop" (Figure 2b). The applied load is changed and then the friction measured again, and so on. This

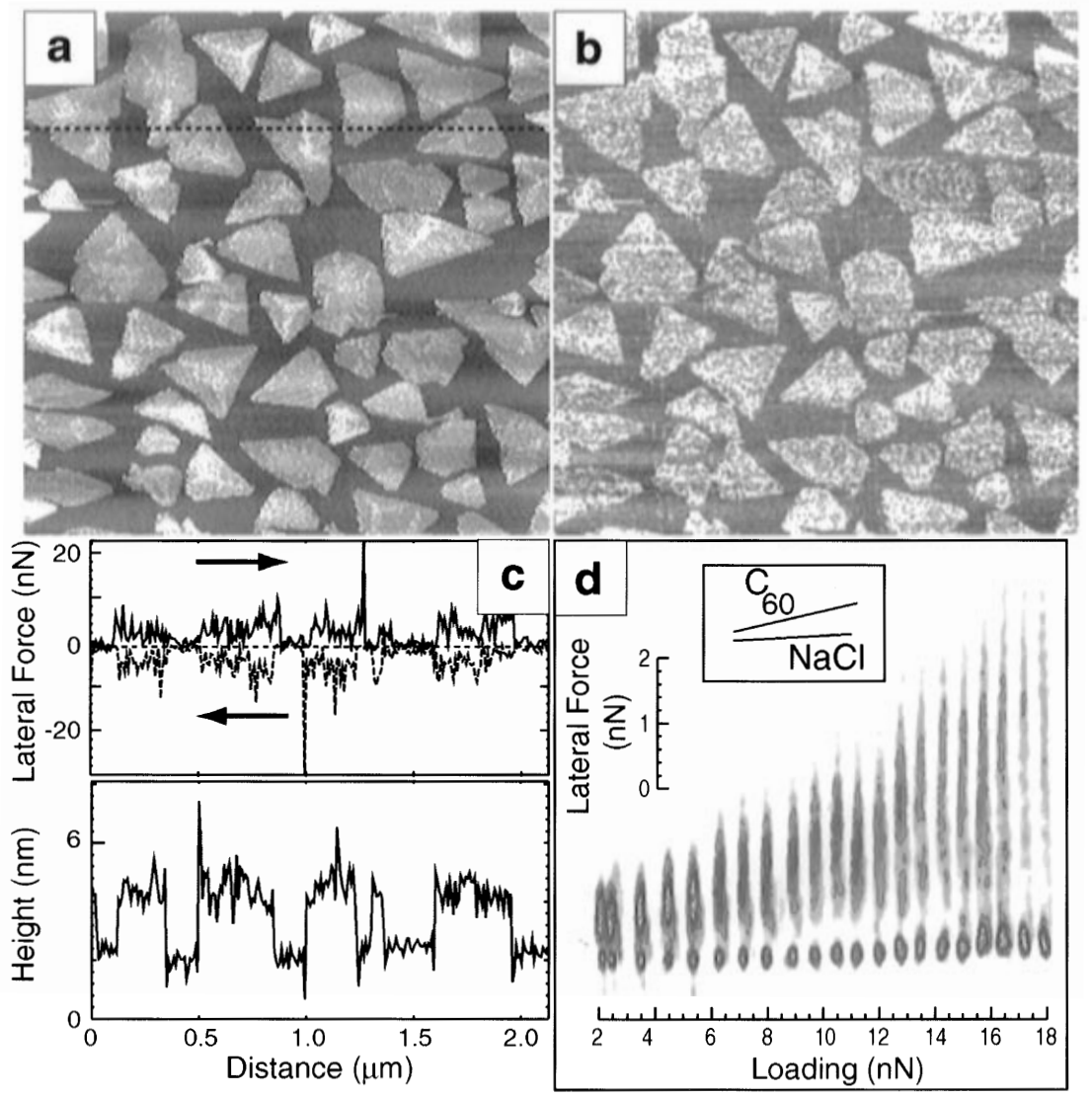

Figure 3. (a) A 2.1 × 2.1 μm^2 topographic image of C_{60} islands on NaCl(001). (b) Corresponding lateral force map. The C_{60} islands appear brighter than the substrate which corresponds to higher friction. (c) Friction loop (upper) and topography (lower) taken along the dashed line indicated in a. (d) The 2D histogram resulting from discrete steps in the load while rastering the tip over the scan area. Two distinct groupings of points are observed. The higher lateral forces correspond to the C_{60} layer, while lower lateral forces correspond to the NaCl substrate. This technique allows frictional properties measured with tips contacting heterogeneous surfaces to be distinguished. (Reproduced with permission from Lüthi *et al.*[70], Copyright 1995 Elsevier Science, B.V.)

produces a so-called friction *vs* load curve.[102] Usually the tip is scanned repeatedly over a limited area to restrict the measurement to one part of the sample at a time. If the sample is heterogeneous, a friction-load measurement should be obtained on each distinct region. Alternately, a large, possibly heterogeneous region of the sample can be scanned while measuring friction and stepping the load for each line of the image. Every load and friction point can then be plotted on a two-dimensional histogram and clustering of the points indicates the friction-load relation inherent to different parts of the sample which are present in the image[70] (Figure 3). This method has the advantage that distinct behavior of different sample regions can be acquired in one image and displayed on one plot. One disadvantage is that, if performed while decreasing the load, the tip will pull out of contact from the region with smallest adhesion first, and regions with larger adhesion will not have friction at the lowest possible loads measured. However, friction could then be easily probed with a separate measurement on the region of interest in such a case. This histogram method will produce some scatter of the data points due to contributions from intermediate regions. It may in fact be desirable to study such contributions, and the method does provide data to explore statistical variations in measured friction forces. Further aspects of friction *vs* load plots will be discussed in sections IV.A.1 and IV.A.2.

3. Force Modulation Techniques

AFM also allows the measurement of local sample elastic properties with unprecedented spatial resolution. There are variations on the exact approach, but the general idea is to use a "force modulation technique"[103−105] to locally investigate Young's modulus of the sample. With the AFM tip scanning in contact with a sample, the relative lever−sample position is modulated vertically and the amplitude of the cantilever's response is monitored. If the sample and tip are very rigid, then the sample

displacement is almost completely transferred to cantilever displacement. However, if the sample is relatively soft, it will undergo significant compression and the amplitude of the cantilever response is reduced (see Figure 4a). As such, relative contrast in the cantilever oscillation amplitude as it is scanned over a surface will reveal differences in the local sample elasticity. Variations on this technique involve measuring the cantilever response as it is brought in and out of contact with the sample, either with a regime of extended tip−sample contact (*i.e.*, acquiring multiple force−distance curves),[106] or only intermittent contact (so-called "tapping mode").[107] To be sensitive to sample properties, the cantilever stiffness must be at least comparable to the sample stiffness. This effectively restricts the technique to polymers, organic thin films, and biological samples if low force constant cantilevers are used. The lateral resolution is limited by the finite contact area formed between the tip and sample. In general, the technique reveals *relative* variations in sample elasticity. An absolute determination of the local elastic modulus is complicated. To do so, the contact mechanical behavior between the tip and sample (contact area, stresses, *etc.*) must be assumed. Usually the Hertz model is used[103−105] but this ignores tip−sample adhesion[106] and viscoelasticity.[108] Nevertheless, many interesting elastic properties of tribologically relevant materials, particularly model lubricants like organic thin films, can be investigated this way and some examples will be discussed further below in section V. This technique has also been applied at ultrasonic frequencies by Kolosov and co-workers.[109,110] The mechanics are quite different since the modulation frequency exceeds the cantilever resonance frequency. As a result, subsurface features become accessible for imaging.

4. Force-Controlled Instruments

Another mode of operation involves displacing the tip by direct application of a force to the tip itself. This requires using a modified AFM where instead of varying the relative lever−sample distance, a force is directly exerted on the tip by some means. Pethica and co-workers[111,112] use a magnetic coating on the tip and external coils to apply forces to the tip. They refer to the instrument as a "force-controlled microscope". Houston, Michalske and co-workers[113,114] control the force electrostatically and refer to the instrument as an "interfacial force microscope". The advantage of the force-controlled techniques is that the tip displacement can be fixed while the load is simultaneously measured. This eliminates the "snap-in" instability that otherwise occurs with AFM when the attractive force gradient between the tip and sample exceeds the normal force constant of the cantilever (Figure 1b).[115−117] One class of experiments that can be performed with this method are hardness measurements. Particularly, the high resolution of AFM allows the hardness and deformation properties of very thin films and small particles to be probed with resolution far beyond that of traditional indentation techniques. These measurements involve exerting loads which are high enough to irreversibly deform the sample. The AFM can be used to cause the deformation as well as to image the affected region afterward.[118,119]

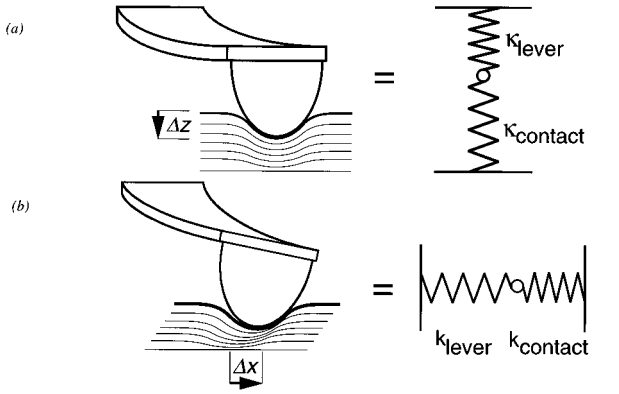

Figure 4. Diagram showing relevant stiffnesses in FFM. Both the cantilever and the contact itself share (a) normal compression Δz and (b) lateral compression Δx. In both cases, the cantilever and the contact act like springs in series. Thus, if one "spring" is much more compliant than the other, it will take up most of the compression. Since the lever deflection itself is measured in the experiment, the relevant lever stiffness must be at least comparable to the corresponding contact stiffness to be sensitive to the contact's elastic properties. (From Carpick *et al.*[125] Copyright 1997 American Institute of Physics.)

Pethica and co-workers have used this method to measure the normal elastic contact stiffness.[120,121] The normal stiffness is given by $\kappa_{\text{contact}} = \mathrm{d}L/\mathrm{d}z$, where L is the applied load (normal force), and z is the elastic penetration depth. Similar to the elasticity measurements described above, an oscillating normal force is applied and the resultant displacement is measured to determine the stiffness absolutely. This measurement is useful because the normal stiffness is related to the contact area and elastic modulus. Unlike conventional AFM, the cantilever displacement is directly controlled and thus a wide range of materials can be sampled.

Solid−liquid interfaces can also be probed with force-controlled techniques. Liquids are known to form solvation layers at solid surfaces. This is obviously an important aspect of actual lubricated contacts which often involve molecularly thin gaps between materials.[32,122−124] An example of a measurement of solvation layers is discussed in section III.A.

5. Lateral Stiffness Measurements

A new operation mode with conventional FFM has been recently proposed and appears to be versatile and of general interest. Similar to the normal stiffness measurement described above, the lateral stiffness of the tip−sample contact, k_{contact}, can be determined.[125,126] An oscillating lateral displacement, $\mathrm{d}x$, is applied and the resultant cantilever torsion, $\mathrm{d}F_{\text{lat}}$, is measured with a lock-in amplifier (see Figure 4b). This measurement of $\mathrm{d}F_{\text{lat}}/\mathrm{d}x$ corresponds to the total lateral stiffness of the system k_{tot} which is given by

$$\frac{\mathrm{d}F_{\text{lateral}}}{\mathrm{d}x} = k_{\text{tot}} = \left[\frac{1}{k_{\text{lever}}} + \frac{1}{k_{\text{contact}}}\right]^{-1} \qquad (1)$$

An additional contribution to the total stiffness may

come from compliance of the tip structure itself.[127] The measurement is useful because the contact stiffness depends upon the elastic constants of the materials and the tip−sample contact area.[125,128] Since typical FFM cantilevers are relatively stiff laterally, the lateral contact stiffness can be sensitively measured for a wide range of materials. The equations for lateral stiffness and an example of such a measurement are presented in section IV.A.2. Note that since the total lateral stiffness k_{tot} is significantly dependent upon the contact stiffness $k_{contact}$, one cannot directly use the slope of the lateral force signal to calibrate the lateral signal sensitivity, which unfortunately has been proposed in the literature.[129]

This ends the description of the essential technical issues and operation modes with the AFM. Instrumental variations for particular applications will be described along with the relevant results.

III. Nanotribology with Other Instruments

To give a wider view into the field of nanotribology, here we will describe briefly the SFA and QCM techniques, each with an example of results, to illustrate their utility and to allow comparison with the capabilities of AFM.

A. The Surface Forces Apparatus (SFA)

The SFA consists of a pair of atomically smooth surfaces, usually mica sheets, which are mounted on crossed cylinders that can be pressed together to form a circular contact under pressure. The mica surfaces can be treated to attach molecules of interest, and the surfaces may be immersed completely within a liquid or maintained in a controlled environment. Actuators attached to either or both of the surfaces' supports are used to apply a load or shear force and to control the distance of separation between them.[32,33] Sensors are attached to measure the load and friction forces. The contact area and relative separation of the surfaces can be measured with optical[130] or capacitive[131] methods. The separation distance can be measured and controlled to the angstrom (Å) level. The lateral resolution is limited to the range of several micrometers. The instrument is thus a model contact where the contacting geometry is known, the material between the surfaces can be varied, and the interaction forces can be controlled and measured. The drawbacks are that the lateral resolution is limited, UHV implementation appears to be extremely difficult, and molecular smoothness is required to obtain meaningful results and so usually the substrate is restricted to mica. Still, many important results have been obtained with this instrument.

For example, the behavior of liquids under compression is of great interest in tribology, and the SFA allows molecular properties to be observed. In Figure 5, the distance of separation, d, between two mica sheets in a liquid medium of octamethylcyclotetrasiloxane (OMCTS) is plotted *vs* the applied load, taken from Frantz *et al.*[131] OMCTS is a simple, nonpolar, low molecular weight Newtonian liquid consisting of quasi-spherical molecules with a diameter of ~0.9 nm. Previous studies have shown that

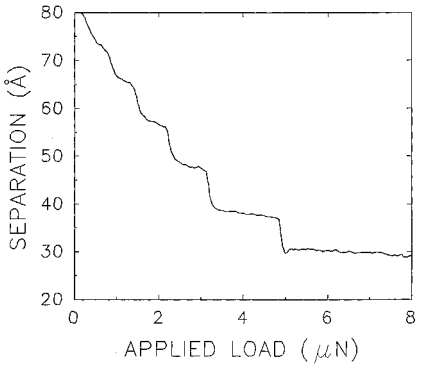

Figure 5. Distance of separation between mica surfaces immersed in OMCTS *vs* applied load as measured with the SFA. Steps in this figure show the layering of the liquid into discrete strata. As the pressure is increased, individual layers are squeezed out. (From Frantz *et al.*[131] Copyright 1996, American Chemical Society.)

under compression, the liquid orders into discrete layers when the surfaces are separated by a small number of molecular diameters.[132] Indeed, as seen in Figure 5, at small separations the smooth decrease in separation as the load is increased (upper left corner) gives rise to a stepwise approach when the number of molecular layers is small. In this regime, steps occur where the liquid has layered and is even able to support a load (a characteristic of a solid). Klein and Kumacheva[133] probed the shear properties of this system, layer-by-layer. They found that, with seven or more molecular layers of OMCTS between the mica sheets ($d \geq 62$ Å), the film responded to shear in a viscous liquid-like fashion (smooth sliding with continuous velocity-dependent resistance). Upon reducing to six molecular layers of separation ($d = 54$ Å), the film underwent an abrupt and reversible transition to solid-like behavior. In this solid-like state the film initially resists shear (no relative motion despite an applied shear force) and then undergoes stick−slip motion. The resistance to shear could be quantified by an "effective viscosity" which was at least 7 orders of magnitude larger than the viscosity of the liquid film that was merely one additional molecular layer thick.

By way of comparison, such layering behavior was also observed with force microscopy. The force-controlled microscope described in section II.D was used by O'Shea *et al.*[121] to investigate the mechanical properties of OMCTS and 1-dodecanol ($C_{11}H_{23}CH_2$-OH) liquids between silicon tips and mica or graphite substrates. With a graphite substrate, both dodecanol (a linear molecule with a polar head group) and OMCTS display stiffness oscillations as the tip−sample gap is varied. This indicates that both liquids are strongly layered near the graphite surface; ~7 solvation layers are detected in each case. Periodic attractive and repulsive forces, correlating with the layered structure, are also observed, providing a quantitative measure of the force required for the tip to penetrate each layer. These experiments demonstrate the sensitivity of force microscopy experiments to liquid structuring and the resultant mechanical properties.

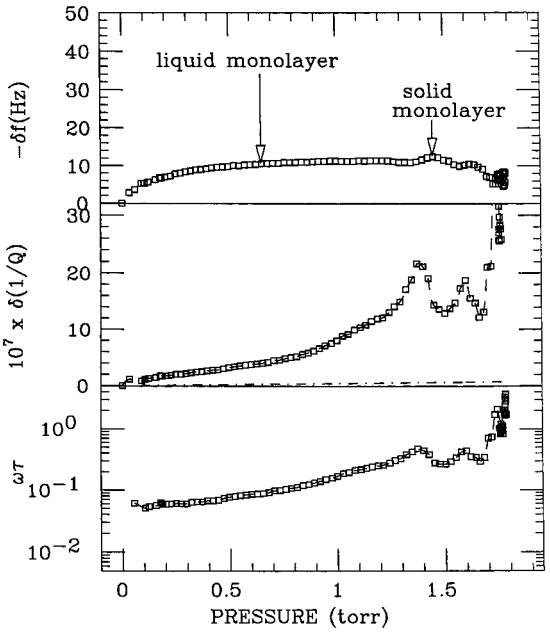

Figure 6. Frequency shift (top), inverse quality factor shift (middle), and slip time (bottom) for Kr adsorption onto a Au surface at 77.4 K. The monolayer film solidifies at ~1.4−1.5 Torr. The solid monolayer has a longer slip time (*i.e.*, slides more easily) than the liquid monolayer. Additional peaks in the data are due to phase transitions. (Reproduced with permission from Krim and Chiarello.[136] Copyright 1991 American Vacuum Society.)

B. The Quartz-Crystal Microbalance (QCM)

The QCM is a familiar tool for monitoring thin film growth with submonolayer sensitivity,[134] since the shift in the resonance frequency of the oscillator is proportional to the mass of adsorbed film. However, Krim and co-workers[28,135] realized that the quality factor of the oscillator decreases if there is slippage of the adsorbed film with dissipative frictional shear forces between the sliding atoms and the substrate (which itself is usually a thin metal film evaporated onto the QCM). From their measurements, they could determine a "slip time"—the characteristic time over which friction acts to reduce the relative motion (thus, a long slip time would imply low friction)—as a function of adsorbate coverage. The slip time is typically of the order of nanoseconds. This temporal sensitivity allows testing of theories of phononic and electronic contributions to friction mentioned above.[21−25] As one interesting example, consider the adsorption of Kr on a Au substrate at 77.4 K.[27,29,136] Figure 6 displays the frequency shift (corresponding to the amount of Kr adsorbed), inverse quality factor shift and the ratio of these two quantities, which corresponds to the slip time, as a function of Kr pressure. As seen in Figure 6, the technique is simultaneously sensitive to energy dissipation as well as coverage changes and associated phase transformations in the film. From this the authors derive the very intriguing result that the solid monolayer structure exhibits longer slip times than the liquid, that is, solid Kr slides more easily on Au than liquid Kr. Modeling and simulations by Cieplak *et al.*[137] indicate that such behavior can be explained by the effect of the structure of the monolayer. In the solid phase, the Kr atoms lock into an ordered structure which is incommensurate with the Au lattice, meaning that the monolayer has essentially no preferred position to occupy, thus it slides easily. This provides an example of the effect of interfacial atomic orientation on friction, a topic we will return in section IV.A in the case of AFM measurements.

From these selected examples, it is clear that a myriad of fascinating and surprising behavior occurs at the atomic/molecular level. The situation is certainly much more complicated, but also much more interesting, than simply measuring a friction coefficient μ.

IV. Bare Interfaces

A. Friction Measurements with Well-Defined Samples

First, we discuss friction force microscopy (FFM), where the normal and lateral deflection of the cantilever are measured simultaneously with the tip in contact with a sample surface. For this review we highlight results on well-defined (*i.e.*, atomically flat and ordered) samples. We divide the discussion into sections relating to different physical aspects of the tip−sample interaction.

1. Atomic-Scale Stick–Slip Behavior

We start our discussion of friction and force microscopy by considering the beautiful yet mysterious phenomenon of atomic-scale stick−slip behavior. Mate *et al.*'s pioneering paper measuring friction with AFM[2] for a W tip on graphite showed that lateral forces exhibited stick−slip behavior with the periodicity of the lattice. Since then, atomic-scale stick−slip behavior has been observed on a wide range of materials: from soft materials like stearic acid crystals (with a silicon nitride tip)[138] to a diamond tip on a diamond surface.[37] Typical atomic-scale stick−slip behavior is shown in Figure 2. Morita et al[51] carried out a systematic study of atomic-scale stick−slip on various materials and discussed the details of the atomic scale slip motions that take place (Figure 7). As seen in parts a and b of Figure 7, both lateral and longitudinal deformation of the cantilever occurs, due to frictional forces acting parallel to the sample surface. By analyzing these signals, the path that the tip traces out across the sample can be determined (Figure 7c). Clearly, on an ordered sample, the tip (whose surface atoms are not necessarily ordered) generally prefers to reside in positions in registry with the sample lattice. (More on the importance of interfacial commensurability will be discussed below.) Note that with the optical beam deflection technique, longitudinal (buckling) deformation of the cantilever cannot be distinguished *a priori* from vertical deflection due to a change in the normal force, since both deflection modes change the angle of the cantilever in the same direction. Thus, one might mistake longitudinal cantilever deformation with a variation in the normal force (particularly if the finite time-constant feedback circuit is operating, since that will smear out a rapid slip into a smoother feedback response). Considering the fact that some coupling between normal and lateral signal channels can also occur with the beam deflection

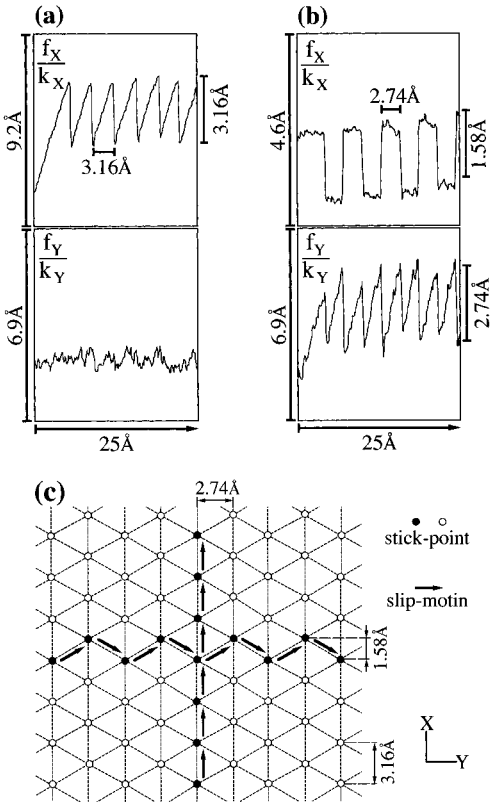

Figure 7. FFM data of lateral lever twisting (f_x/k_x) and longitudinal buckling (f_y/k_y) due to frictional forces parallel to the MoS_2 surface acting on a silicon nitride tip. The long axis of the lever is along the *y* axis. In a, the lever was scanned along the *x* direction indicated in c; *i.e.*, perpendicular to its long axis. Stick−slip behavior resulted in periodic lateral twisting of the lever, and no appreciable back-and-forth longitudinal buckling of the lever. In b, the lever was scanned along the *y* direction indicated in c; *i.e.*, parallel to its long axis. This time, the lever buckled longitudinally forward and back (top) and twisted back and forth (bottom) as it was scanned. This allowed the individual stick points and the path of the tip to be mapped out, as indicated in c. The stick points corresponded to the MoS_2 unit cell. (Reproduced with permission from Morita *et al.*[51] Copyright 1996 Elsevier Science B.V.)

scheme,[62,70] we propose that this periodic lateral force interaction is responsible for *all* atomic-lattice contrast images obtained with *contact* AFM, including topographic images. To our knowledge, no observation of atomic lattice contrast *without* atomic-scale stick−slip behavior has yet been reported, while lateral force atomic lattice contrast, when it is measured, is often clearer than normal force contrast.[139] In general, one must not imagine the AFM tip smoothly tracing out individual atomic corrugations akin to an STM, but instead realize that the relative tip−sample motion is *discontinuous* and involves a multiple-atom contact area.

The term "stick−slip" must be used with caution: in general "stick−slip" refers to behavior of a macroscopic contact involving multiple contact asperities. For example, a creaking door hinge, a bowed violin string, screeching tires, and earthquakes are all examples of macroscopic stick−slip behavior. Furthermore, stick−slip in micrometer-sized single asperity contacts with molecularly thin interlayers has been observed in SFA experiments.[140] A rich variety of phenomena are involved in these examples,[7] but the unifying principle is that the frictional force depends upon the relative tip−sample sliding velocity. Specifically, friction during sliding is lower than the friction when not sliding. If a constant stress is applied to an interface that is stuck together, then when the applied stress exceeds the static friction, sliding occurs and so friction is now lower. Initially, this leads to increasingly faster relaxation of the applied stress until it is no longer large enough to maintain sliding. The system is then "stuck" again and the cycle repeats itself. The behavior is influenced to varying degrees by factors such as the roughness/topology of the contacting surfaces, "creep"/strengthening of the interface during sticking, and velocity dependent effects particularly with viscous or viscoelastic materials. With AFM we are dealing exclusively with "atomic-scale stick−slip". In contrast to macroscopic stick−slip, the interface is atomically smooth, wear does not appear to occur, and the contact involves only solid, elastic materials.

Several theoretical efforts to explain and model atomic-scale stick−slip behavior, specifically in the context of force microscopy have appeared in the literature. These can be divided into semiclassical simulations/calculations,[141−153] and molecular dynamics simulations.[154−160] Primarily the semiclassical models attempt to explain the *mechanics* of stick−slip behavior. The starting point for these models is the Tomlinson model proposed more than five decades ago.[161] Some of these model the tip as a single atom or at least a single entity without internal degrees of freedom,[141,146−148,151,152] although multiple atom tips have also been considered.[142,150,153] Consistent with experimental results, a periodic interaction potential is assumed to exist between the tip and sample. In most cases the scanning process is carried out adiabatically, *i.e.*, the system is assumed to be in equilibrium at each step of the simulation, since typical AFM scanning velocities are much smaller than the sound velocities of the materials. When scanning, the lateral displacement between the lever and the sample is increased. The tip initially resides in a potential minimum that is determined by the tip−sample interaction. Finite static friction due to the tip−sample interaction inhibits sliding of the tip, and so elastic energy is built up in the cantilever and, as Colchero *et al.* have appropriately pointed out,[152] in elastic deformation of the tip and sample themselves (Figure 4b). The total energy of the system consists of the interaction energy and the elastic energy stored in the lever and the contacting materials (see Figure 8). Eventually a critical point is reached where the elastic strain energy eliminates the potential minimum. Relative slip between tip and sample then takes place. The lever and the contact quickly relax, releasing energy, and the motion is brought to a stop as the tip finds a new potential minimum, one unit cell over. The phonons generated in this process in the tip and sample are assumed to carry energy away from the interaction region; energy has thus been dissipated. Since phonon frequencies are much higher than typical AFM scanning frequencies (by a factor of $\sim 10^{12}$), this relaxation occurs very quickly. All the models produce atomic-scale stick−slip behavior, including the

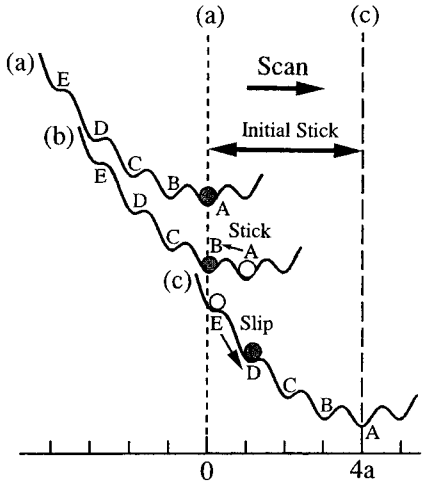

Figure 8. One-dimensional schematic illustration of the total energy V (vertical axis) *vs* displacement for an AFM during scanning, assuming a single point potential for the tip−sample interaction (*i.e.,* a single atom tip). The atomic periodicity of this interaction is superposed on the parabolic elastic strain energy due to cantilever bending and elastic contact strain. The cantilever is located at (a) $x = 0$, (b) $x = a$, and (c) $x = 4a$. a is assumed to be one lattice constant. Dotted and broken lines perpendicular to the x axis correspond to the case for (a) $x = 0$ (initial lever position) and (c) $x = 4a$, respectively. The filled circle represents the tip "atom". A, B, C, and D are metastable points ($\partial V/\partial x = 0$, $\partial^2 V/\partial x^2 > 0$). E is an unstable point, where $\partial V/\partial x = \partial^2 V/\partial x^2 = 0$. Slip from E to D takes place at this point in the scan. (Reproduced with permission from Sasaki *et al.*[146] Copyright 1996 Japanese Journal of Applied Physics.)

models of Gyalog *et al.*[145,148] and Hölscher *et al.*[147] which are carried out dynamically (by solving the equations of motion). The collective results of these semiclassical models are as follows:

·The atomic-scale stick−slip instability can be interpreted as the system (tip and sample) residing in or searching for total potential energy minima, where the energy is the sum of the tip−sample interaction potential and elastic energy stored in the cantilever and contact

·Weak cantilever springs and compliant contacts, together with strong tip−sample interactions are required to produce the atomic-scale stick−slip instability. It has been suggested that if this is not the case, then this instability can be prevented and frictionless sliding can occur.[141,143,158,162,163] However, this neglects other velocity-dependent forms of frictional dissipation, such as electronic contributions.[21−25]

·The atomic-scale stick−slip periodicity reflects the periodicity of the interaction potential.

·The two-dimensional stick−slip effects observed in experimental images can be reproduced in these simulations,[144,146,147,149,151,164] including observable effects in the images due to anisotropy in the cantilever spring constants (lateral *vs* longitudinal).[144,146,148,149,151]

·The energy dissipated will be distributed among the substrate, tip and cantilever depending on their relative stiffness,[152] with the more compliant components dissipating more energy.

Further insights are provided by molecular dynamics simulations. Atomic-scale stick−slip has been predicted in several simulations. For example, ordered hydrogen-terminated diamond surfaces sliding together was modeled by Harrison and co-workers.[154,155] They observed that the stick−slip behavior varied with applied load, scan speed and scan direction with respect to crystallographic directions. Landman and co-workers[159,160,165] simulated a Si tip/surface pair. Wearless atomic stick−slip occurred for low applied loads. Interestingly, a periodic lateral force was observed even if the tip was disordered. All of these simulations provide local pictures of the vibrational motion and energy dissipation generated during atomic stick−slip motion, showing that excitations are highly localized in the contact zone.

Sørensen *et al.*[156] simulated Cu tips sliding on Cu surfaces. Wearless atomic stick−slip occurred for a (111)-terminated tip sliding on a (111) surface. The bottom layer of the tip (9×9 atoms) were shown to slip via a dislocation mechanism. The tip atoms initially reside in surface fcc positions. During the rapid slip, tip atoms start to jump from fcc to hcp sites to relieve lateral strain. The slipped and unslipped atoms are separated by a dislocation which propagates through the contact. Variations with scan velocity and relative orientation were also probed. Friction was observed to decrease with increasing scan velocity. At higher velocity, more phonons are excited during a slip and can promote subsequent slip events.

The lack of experimental control or even knowledge of the tip atomic structure makes comparison with these simulations challenging but not impossible. More serious may be the gap in timescale and velocity of these simulations—typical MD simulation velocities are 10^0-10^2 m/s *vs* typical AFM experimental velocities of 10^{-7} to 10^{-5} m/s. In this sense, sophisticated versions of the "quasi-static" simulations described above are desirable.

At this point, let us consider some aspects of the experimental results. First, there has not been any clear experimental conclusions indicating under exactly what conditions does stick−slip occur. Often, well-resolved images like the one shown in Figure 2a are not obtained; yet, under the same loads, with the same sample and with the same cantilever, some unknown change in the tip occurs and regular stick−slip is observed. The reasons why stick−slip is observed at some times and not others is not understood. Does friction vary with load in the same manner whether or not stick−slip is observed? Furthermore, larger scale stick−slip behavior is observed in SFA experiments[166−168] but a transition to smooth wearless sliding occurs at higher velocities. No reports of stick−slip to smooth sliding transitions have been made with FFM, probably due to FFM's limited scan speeds. This limit should be quantified and faster FFM experiments attempted.

Also unresolved is the question of stick−slip periodicity. Most accounts of stick−slip motion so far, report *one* stick−slip event per surface unit cell, even when the unit cell contains more than one atomic species, such as alkali halide surfaces, including KBr[164] and NaF.[51,169] One exception is the large unit cell of Si(111)7×7 measured in UHV with tips coated with polytetrafluorethylene[139] where multiple stick−slip events per unit cell were resolved. With KBr, Giessibl and Binnig[170] resolved both K^+ and Br^- ions in the normal force signal in UHV at 4.2 K, so

perhaps two stick−slip events per unit cell were taking place (lateral forces were not measured in this experiment). Yet Lüthi *et al.*[164] observed only one stick−slip event per unit cell at room temperature with KBr in UHV. What then determines the periodicity of stick−slip behavior? Furthermore, are all the interfacial atoms participating in periodic motion, or only a fraction of them? More experimental results and further theoretical efforts should address this problem.

If FFM measurements involve stick−slip motion, then we must keep in mind that we are dealing with *static* friction. The force of interest is thus the lateral force for which the tip slips across the surface, *i.e.*, the *maximum* force measured in a stick−slip plot like that shown in Figure 2b. Many FFM studies calculate the *average* friction force instead. We propose that the distinction between these quantities needs to be explicitly stated by experimentalists when reporting friction data.

2. Properties of a Single Asperity: Interfacial Friction

Real surfaces are rarely perfectly smooth.[18,19] Rather, the interface between two materials in "contact" will actually be composed of a small number of contacting asperities, and the real contact area is much smaller than the apparent contact area. The mechanical properties of these small asperities can differ substantially from bulk properties. To understand the behavior of such a complex contact, it is desirable to learn about the properties of a single asperity.

Recent FFM experiments have indicated that the FFM tip can form a single asperity contact with the sample surface.[85,102,171−174] The measurements can be performed in the low load regime where the tip−sample interaction during frictional sliding is believed to be completely elastic (*i.e.,* without wear). This is often referred to as "interfacial friction".[175,176] This opens up the possibility of applying and testing existing theories of continuum contact mechanics with the properties of a nanometer-scale single asperity. The shear strength and the work of adhesion are two important physical parameters one can measure. The shear strength corresponds to the shear force per unit area (or per atom) required to shear the interface (*i.e.*, cause slip in the stick−slip regime). The work of adhesion corresponds to the energy per unit area (or per atom) required to pull apart the interface. These quantities could be considered, respectively, the fundamental friction and adhesion parameters of an interface, and could be compared to modeling and theory. The primary questions to be resolved include: how do these quantities depend upon the atomic structure and chemical composition of the interface? the applied pressure? the temperature? Experiments used to obtain such measurements will be described below.

First we briefly review the concepts of continuum contact mechanics; references are provided for further details. Given a contact geometry and applied load, contact mechanics allows the determination of the stress distribution, elastic indentation depth, and contact area.[128] The original theory was due to Hertz,[177] who showed that for a sphere−plane contact, the load-dependence L of the contact area A is given by

$$A = \pi\left(\frac{R}{K}L\right)^{2/3} \tag{2}$$

where R is the radius of the sphere and

$$K = \frac{4}{3}\left(\frac{1-\nu_1^{\,2}}{E_1} + \frac{1-\nu_2^{\,2}}{E_2}\right)^{-1} \tag{3}$$

with E_1 and E_2 the Young's moduli of the sphere and plane, respectively, and ν_1 and ν_2 the Poisson's ratio of the sphere and plane, respectively. In the case of FFM, the plane corresponds to the sample and the sphere corresponds to the tip. The contact area is important because we may expect the friction force F_f to be proportional to the contact area:[16]

$$F_f = \tau_0 A \tag{4}$$

where τ is the interfacial shear strength, *i.e.*, the frictional force per unit area. Proportionality between friction and contact area has been observed for elastic, wearless, single asperity contacts in SFA experiments.[176,178] The shear strength may be a constant, or perhaps it might have a pressure (P) dependence:

$$\tau = \tau_0 + \alpha P \tag{5}$$

as observed for example in SFA experiments with Langmuir−Blodgett monolayer films between mica surfaces in contact,[179] and suggested by the recent theoretical models of Sørensen *et al.* of a Cu tip on a Cu surface.[156] Here, a linear dependence on pressure is merely assumed, with τ_0 and α assumed to be constants; however, a more complicated dependence may exist.

The Hertz theory assumes that no attractive forces act between the two materials, whereas AFM experiments often reveal substantial adhesion between the tip and sample, and therefore eq 2 must be modified. In other words, the finite interfacial adhesion energy must be taken into account. Adhesion is included in the contact mechanics theories of Johnson, Kendall, and Roberts (JKR)[180] for the case of short-range adhesion between relatively soft materials, and Derjaguin, Müller and Toporov (DMT) for long-range adhesion between harder materials.[181] The DMT description corresponds to the Hertz description with the normal force shifted by the total adhesion force. Descriptions of the transition between these limits are provided by Müller *et al.*,[182] Maugis,[183] and Johnson and Greenwood.[184] Contact area *vs* load curves are sketched in Figure 9 for each of these cases. Capillary condensation is present in FFM experiments carried out in air, and this situation is considered by Fogden and White (FW)[185] and in a noteworthy addendum in Maugis' paper.[183] All of these models neglect the effect of lateral forces on the contact. This problem is complicated to model but a recent paper by Johnson[186] presents an analytical model that appears to be consistent with available experimental data (including AFM results).

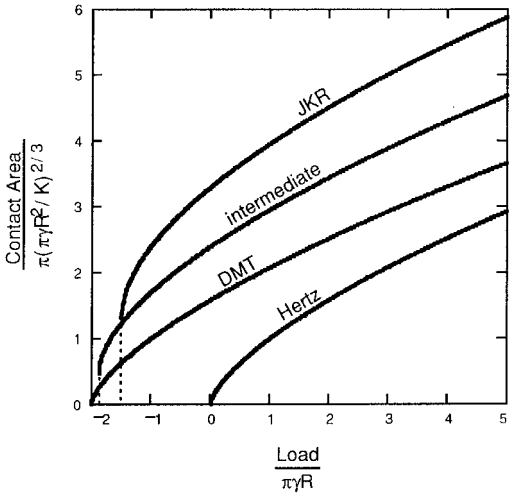

Figure 9. The JKR−DMT transition. The exact relationship between contact area and load for an elastic sphere contacting a plane depends upon the range of attractive surface forces. Area−load curves for the JKR limit (short-range adhesion), the DMT limit (long-range adhesion), and an intermediate case are shown. All of these approach the Hertz curve in the limit $\gamma \rightarrow 0$ (no adhesion). Load and area are plotted in nondimensional units as indicated. Adhesion increases the contact area from the Hertz case for a given load by an amount dependent upon the range of attractive forces.

To interpret a measurement of friction *vs* load, one of the above contact area models, along with a model for the shear strength, must be chosen and fit to the friction data. To extract quantitative information, the elastic constants of the tip and sample must be known, along with the shape and dimensions of the tip. Forces must be accurately calibrated too, as discussed above. Not all of these requirements are met in the experiments described below and so some of the numerical results are subject to substantial uncertainty.

However, the recent development of the lateral stiffness technique described in section II.D.5 allows the contact area to be determined experimentally.[125] The lateral stiffness of an elastic contact between a sphere and a plane is given by[128]

$$k_{\text{contact}} = 8G^*a \qquad (6)$$

where a is the contact radius and $G^* = [(2 - \nu_1)/G_1 + (2 - \nu_2)/G_2]^{-1}$. Here G_1 and G_2 are the tip and sample shear moduli, respectively. This assumes that no slip takes place at the interface. In the experiment, one measures the total system stiffness, k_{tot}, given by eq 1. Extracting k_{contact} from this measurement therefore produces a quantity proportional to the contact radius. This new approach then allows the frictional contributions of contact area and shear strength to be separated. If the elastic constants of the materials are known, then the contact area can be determined. Conversely, a model for the contact area can be fit to the data to extract values for the elastic constants, namely G^*.

This technique was used by Carpick *et al.* for silicon nitride tips in contact with mica in air (at 55% relative humidity).[125] They found that the contact area varied with load in a DMT-like fashion, in accordance with the FW prediction for saturated

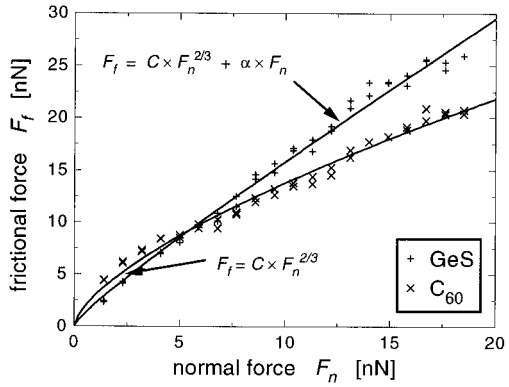

Figure 10. Friction *vs* load for a Si tip on GeS and C_{60}. The data points represent averages from friction images taken at different loads. The solid lines represent fits to the data discussed in the text. Notice that, at low loads, the C_{60} film exhibits higher friction, but at higher loads the GeS substrate exhibits higher friction. (Reproduced with permission from Schwarz *et al.*[174] Copyright 1995 American Physical Society.)

capillary condensation, and also that the shear strength was constant over the load range examined (±40 nN). Assuming the bulk values for the elastic constants, they determined a value of ~680 MPa for the shear strength.

All previous shear strength determinations did not directly measure the contact radius, but instead relied on contact mechanical models as described above to determine the contact area. Schwarz *et al.* measured friction *vs* load in ambient air (RH ~55%) with a Si tip (with most likely a SiO_2 termination) on C_{60} islands grown on a GeS substrate.[174] Since the C_{60} coverage was incomplete, they performed with the same tip, friction measurements on both the GeS and the C_{60} surfaces together. Their results are shown in Figure 10. The load data are shifted by the pull-off force which was 6.7 nN. Remarkably, the friction contrast reversed at ~7 nN total normal force (0.3 nN external load). Below this load, the SiO_2/C_{60} interface exhibited higher friction, while at high loads, the SiO_2/GeS interface exhibited higher friction. Clearly, distinct functional dependences of friction upon load were being observed. Friction between the tip and GeS was nearly linear with load, while between the tip and C_{60}, the dependence was closely proportional to $L^{2/3}$. The authors postulated a pressure-dependent shear strength, *i.e.*, that eq 5 above applied. Combining eqs 4 and 5 gives

$$F_f = \tau_0 A + \alpha L \qquad (7)$$

Assuming the contact area was varying in a DMT fashion, as might be expected from the FW theory, they could estimate τ_0 and α for these pairs of materials. Unfortunately, the tip radius was not measured nor the tip shape checked, and the elastic constants were uncertain. With several adjustable parameters, there is some uncertainty in the fitting. Nonetheless, using what they felt were reasonable estimates, the authors quote values for the best fits, which are reproduced in Table 1.

Meyer *et al.* applied contact mechanics models in their studies of highly stepped NaCl(001) surfaces with Si tips in a dry nitrogen atmosphere.[173] They

Table 1. A Comparison of Shear Strengths and Adhesion Energy Measurements by Various Techniques for Certain Interfaces

materials in contact	environment	shear strength (Pa)	adhesion energy (J/m^2)	ref
		AFM Results		
SiN tip/mica	air, ~55% RH	6.8×10^8	determined by capillary formation	125
Si tip/$C_{60\ islands}$	air, ~55% RH	$\tau = \tau_0 + \alpha P$: $\tau_0 \approx 3.3 \times 10^9$, $\alpha \approx 0$	determined by capillary formation	174
Si tip/GeS		$\tau = \tau_0 + \alpha P$: $\tau_0 \approx 1.2 \times 10^9$, $\alpha \approx 1.1$; or $\tau_0 = 0$, $\alpha \approx 1.5$		
Si tip/NaCl: terraces	dry N_2	9.6×10^7 (JKR) 1.45×10^8 (extended JKR)	0.027−0.035[a]	173
steps		1.42×10^8 (JKR) 4.78×10^8 (extended JKR)		
Pt-coated tip/mica	UHV	9.1×10^8 max,2.7×10^8 min	0.404 max, 0.019 min	172
C_{60}/NaCl	UHV	$(0.5-1) \times 10^5$		188
MoO_3/MoS_2	dry N_2	1.1×10^6		189
Cd−arachidate/Cd−arachidate	ambient	$(1.0 \pm 0.2) \times 10^6$		190
		SFA Results		
mica/mica	dry air	2.5×10^7		178
mica/mica	dry air/N_2		0.123−0.157[b]	191
fatty acid monolayers−$(C_{n-1}H_{2n-1})$-COOH between Mica sheets	ambient	$\tau = \tau_0 + \alpha P$:		179
$n = 141$(myristic acid)		$n = 14$: $\tau_0 = 6 \times 10^5$, $\alpha = 0.034$		
$n = 18$ (steric acid)		$n = 18$: $\tau_0 = 6 \times 10^5$, $\alpha = 0.038$		
$n = 221$(behenic acid)		$n = 22$: $\tau_0 = 22 \times 10^5$, $\alpha = 0.048$		
		QCM Results[c]		
Kr monolayer/Au(111)	UHV	5×10^{-1}		136
		Macroscopic Results		
SiO−Cu-bonded interface	*d*	$(0.56-1.67) \times 10^9$		192
glass/stearic acid/Al	ambient	$\tau = \tau_0 + \alpha P$: $\tau_0 = 5.8 \times 10^6$, $\alpha = 0.068$		193
MoS_2-sputtered films on hard substrates	dry air	$\tau = \tau_0 + \alpha P$: $\tau_0 = 2.48 \pm 0.5 \times 10^7$, $\alpha = 0.001 \pm 0.001$		194

[a] Calculated by present authors based on information in reference. [b] Immediately after cleavage. Adhesion decreases substantially with time due to adsorption of contaminants. [c] QCM measurements are performed at much shorter time scales than AFM and SFA experiments. [d] This experiment measured the ultimate interfacial shear strength for a thin film of silica deposited onto a copper substrate with a stress-induced cracking technique.

observed that friction was enhanced at step edges and varied nonlinearly with load both on the flat terraces and in the vicinity of steps. Their data were fit best by using the JKR theory with distinct pressure-independent shear strengths for the steps and terraces. Results are shown in Table 1 and come from either a regular JKR fit or an "extended" JKR fit of the combined frictional effect of the terraces and steps since the tip is never in contact with just the step edge atoms by itself.

Carpick *et al.* measured friction *vs* load with a Pt-coated tip in contact with mica in UHV.[85] They observed that friction varied with load in proportion to the JKR predictions of the contact area (Figure 11a). They confirmed the shape of the tip and measured its radius by scanning it over a sharp feature on the surface of $SrTiO_3$.[187] Furthermore, by deliberately altering the tip shape (Figure 11c), they observed that the frictional behavior changed according to the JKR prediction for the modified tip shape (Figure 11b). These results demonstrate that, without knowledge of the tip shape, the functional dependence of friction upon contact area is ambiguous. The knowledge of the tip shape and size allowed the shear strength and adhesion energy to be determined to within the accuracy of the lever calibration. The authors also observed a progressive reduction of the adhesion energy and shear strength each time the tip was scanned in contact with the mica (Figure 12). Overall, the adhesion energy dropped by a factor of 20 and the shear strength by a factor of 3. The results are summarized in Table 1. The friction and adhesion reduction was caused by chemical and structural modification of the tip, possibly by adsorption of K^+ ions from the mica surface to the tip which would lower the surface free energy of the Pt.

The above examples illustrate that frictional properties specific to the materials in contact and the interfacial chemistry can be observed and quantified using the FFM tip as a single asperity probe.

Uncertainties about the tip shape and composition can be overcome by using the tip to cause relative sliding of a *different* interface formed between islands of one material on top of another. Three examples of these important measurements are given here. Lüthi *et al.*[188] used the FFM tip to push C_{60} islands across the surface of NaCl in UHV. Since the island size could be imaged by the AFM in topographic mode, the contact area between the C_{60} and NaCl could be determined, as could the critical shear force necessary to initiate relative motion. They determined a shear strength of 0.05 to 0.1 MPa. Sheehan and Lieber[189] used the FFM tip to slide MoO_3 islands across a MoS_2 substrate in a dry N_2 environment. They observed that shear occurred only in preferential directions (discussed further below). Shearing

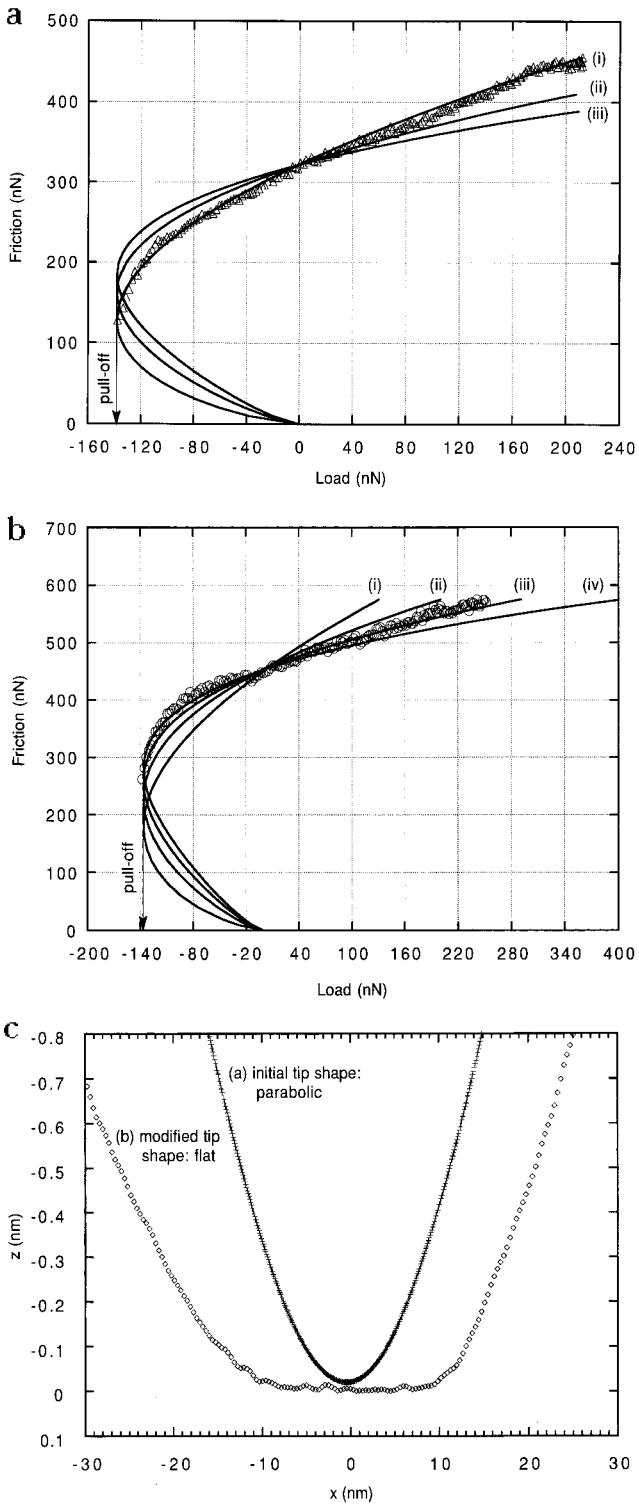

Figure 11. Friction *vs* load plots for a Pt-coated tip in contact with mica in UHV. (a) Friction *vs* load data (triangles) and JKR prediction for increasingly flatter tip shapes (solid lines): (i) parabolic, $z \propto r^2$; (ii) $z \propto r^4$; and (iii) $z \propto r^6$. The data initially follow the JKR prediction for a parabolic tip (solid curve i). (b) After blunting the tip by applying large loads, the friction (circles) varies with load according to a modified JKR description for a flatter tip shape. The solid lines represent the same tip shapes described in a with curve iv $z \propto r^8$ added for further comparison. (c) Tip cross-sections confirm that in a the tip was nearly parabolic and in b the tip was flatter. (Adapted from Carpick *et al.*[85] Copyright 1996 American Vacuum Society.)

islands of different sizes confirmed a shear strength of 1.1 MPa, roughly independent of the island size.

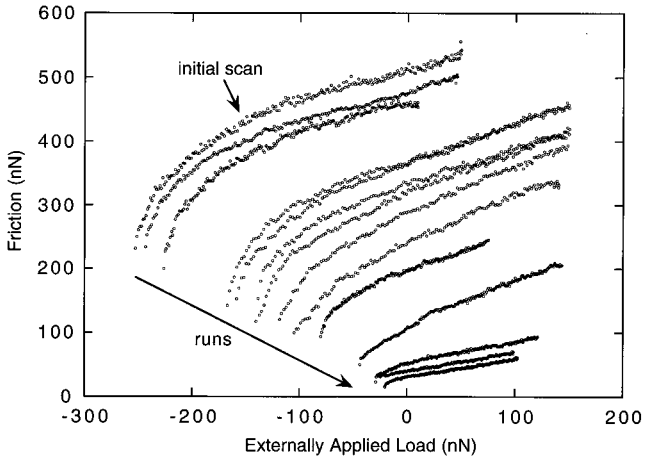

Figure 12. Scanning-induced reduction of adhesion energy and shear strength is revealed by friction *vs* load plots for a Pt-coated tip in contact with mica in UHV. After each plot, the pull-off force decreased in magnitude, implying a scanning-induced decrease in the adhesion energy. Curve fitting reveals that the shear strength also decreased. This implies that changes in the structure or chemistry of the interface can dramatically affect friction and adhesion. This behavior occurred independently from the tip shape alterations described in Figure 11. (From Carpick *et al.*[172] Copyright 1996, American Chemical Society.)

Meyer *et al.*[190] used the FFM tip to slide an island of a Langmuir−Blodgett (LB) film, Cd−arachidate, across an underlying Cd−arachidate layer on a Si substrate. The shear strength was determined to be 1.0 ± 0.2 MPa. Details of the special properties of LB films will be discussed in section V.

These examples are the first observations of shear strengths at this level. These results are summarized in Table 1, with measurements obtained by different techniques included for comparison.[136,178,179,191−194] Note the wide spread in shear strength values, which has been discussed briefly by Krim.[4] More experiments, particularly in a controlled environment like UHV, are needed to establish trends.

The macroscopic friction coefficient has not entered into this discussion. As mentioned in the introduction, direct proportionality between friction and load is a consequence of multiple-asperity contact[18,19] and wear[20] or plastic deformation.[15] If friction is observed to scale linearly with load in a FFM experiment (which has been reported in several cases), then either the contact is not a single asperity, the shear strength is pressure dependent (as suggested by Schwarz *et al.*,[174] as described above), the contact is not wearless, or some as-yet-unknown process is responsible. Simply listing a value for a friction coefficient fails to provide insight into the fundamental mechanisms of friction. Friction coefficients reported with FFM will thus not be emphasized here since they are, as stated by Krim, of "relative insignificance concerning how friction originates".[4] Furthermore, without specifying more about the interface (*e.g.*, tip size and shape), it is impossible to reliably compare measurements made by different FFM experimenters if only a friction coefficient is mentioned.

Connecting *macroscopic* friction coefficients with single asperity friction measurements is not an

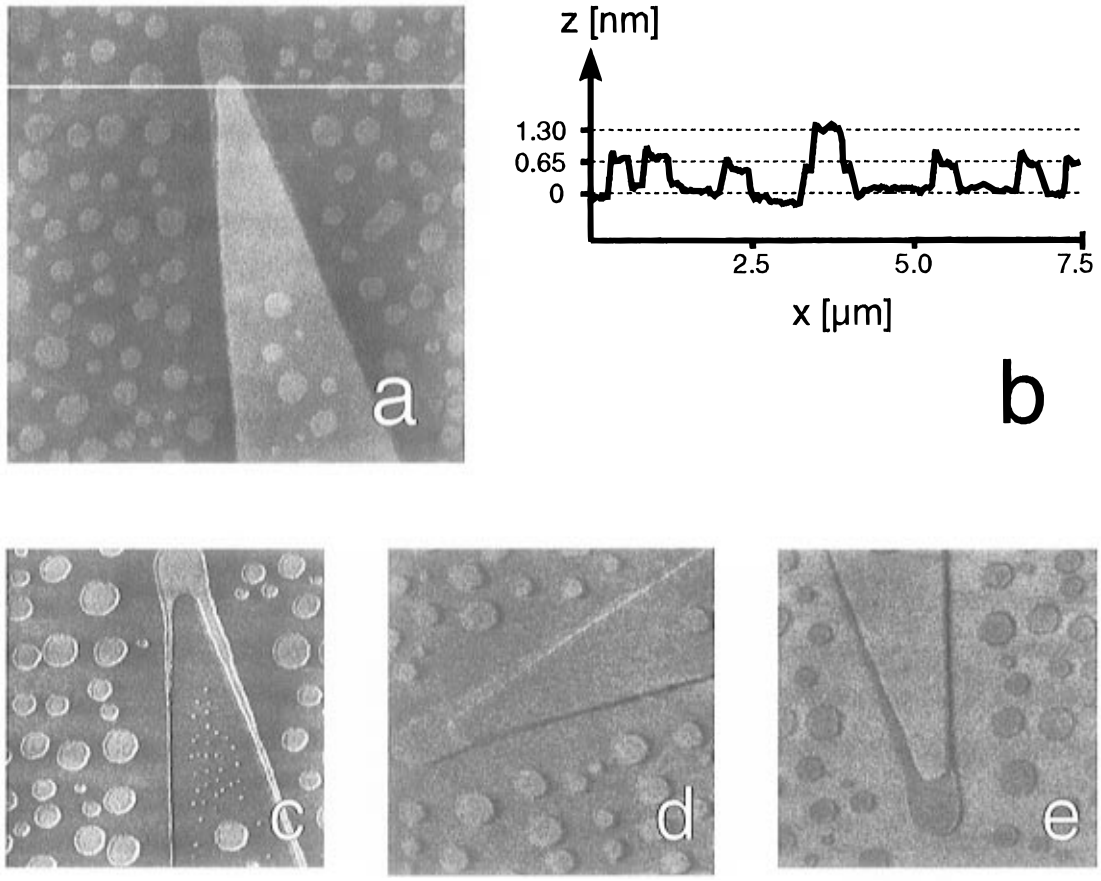

Figure 13. (a) A 7.5 × 7.5 μm^2 topographical image of the surface of a negative domain of TGS. A cleavage step and islands originating from a recrystallization process are visible. The single steps have a half-unit cell height. (b) *z*-profile taken along the line indicated in a. Remaining images depict left-to-right friction force scans with the sample rotated by (c) 0°, (d) 90° and (e) 180° with respect to the orientation shown in a. The friction contrast is seen to reverse between c and e, and is minimal in d. The *a* axis of the crystal is along the vertical direction. (Adapted with permission from Schwarz *et al.*[197] Copyright 1996 Kluwer Academic Publishers.)

impossible task, and in fact can be worked out somewhat generally for rough surfaces in elastic contact.[18,19,195] More complicated situations, particularly mixed elastic−plastic conditions, can also be modeled and in fact require knowledge of single asperity friction parameters as inputs. The data obtained in these FFM experiments are clearly useful for accomplishing this task. We will return to this consideration in our Conclusions, section IV.

Finally we note here that the analysis of the above results assumes that no wear is taking place. While indeed no wear is observed in these experiments, unobservable point defects may be created in the sliding process. We will discuss this possibility further in section IV.B.1.

3. Frictional Anisotropy

Another unsolved problem in nanotribology is the directionality dependence of friction (does slip occur more easily in particular crystallographic directions?). The following examples demonstrate that the tip−sample frictional interaction can depend upon the molecular/atomic orientation and structure of the interface in a measurable fashion.

Bluhm *et al.*[196,197] reported frictional anisotropy depending on the scan direction of a FFM tip on the surface of triglycine sulfate (TGS). TGS is a ferroelectric crystal, thus possessing positive and negative domains. Each domain produces two cleavage surfaces which are chemically equivalent, but structurally rotated by 180° with respect to one another. Within a given domain, one sees terraces separated by half-unit cell step heights corresponding to these two cleavage surfaces. Figure 13a shows a topographic image of the negative domain exhibiting such steps. Friction scans of the same area, Figure 13, parts c, d, and e, show unique behavior: the frictional contrast between the two terminations depends upon the scan direction with respect to the crystallographic axes, and in fact reverses if the orientation is changed by 180°. In between the contrast is almost zero. A similar effect was seen on positive domains. The maximum directionality contrast was ∼3−4% of the total friction force. Given the 180° relation between the two cleavage surfaces, this means that friction is higher when scanning parallel to a particular molecular structure, and lower when scanning antiparallel to that structure (see Figure 14 for details). Similarly, frictional anisotropy was observed by Overney *et al.*[198] for a silicon nitride tip sliding on a lipid bilayer film on a Si substrate. This film possessed domains of distinct molecular orientations which provided frictional contrast (by a factor of ∼1.4:1) that depended upon the scan direction.

In the experiment of Sheehan and Lieber[189] where the FFM tip was used to slide MoO_3 islands across a MoS_2 surface, they observed that the MoO_3 islands would slide exclusively along low index MoS_2 lattice

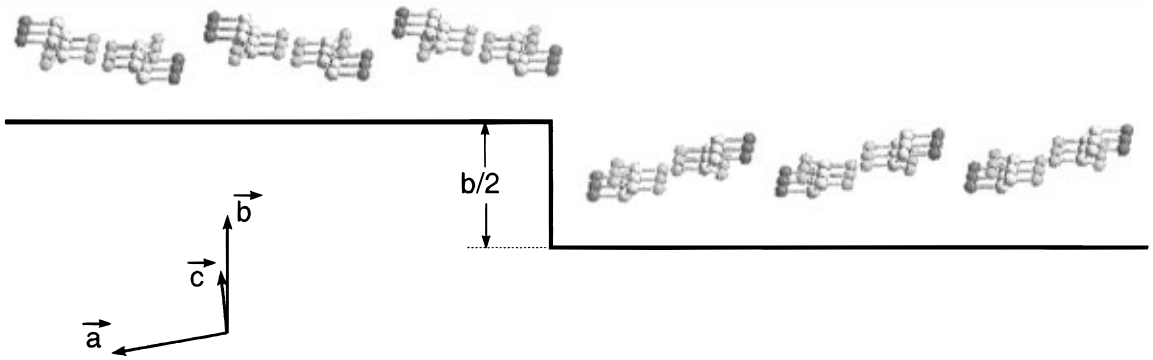

Figure 14. Perspective view of the negative domain surface of TGS exhibiting a surface step of half of the unit cell height. The structure consists of glycinium molecules (NH_3CH_2COOH; H atoms not shown in figure) forming a sawtooth-like structure perpendicular to the *c* axis. The structure on the lower terrace is rotated by 180° around the *b* axis with respect to the molecules on the upper terrace. The entire TGS structure is provided in ref 197. (Reproduced with permission from Schwarz *et al.*[197] Copyright 1996 Kluwer Academic Publishers.)

directions, namely the {1000} family of directions. They could not slide the islands in other directions. The work of Morita at al.[51] tracing out the path the FFM tip follows across mica, MoS_2, or NaF surfaces, shows that the FFM tip itself strictly follows preferred directions when sliding (see Figure 7c). From these examples, we see that the relative atomic or molecular orientation of surfaces in contact can play a critical role in determining friction. Significantly, the theoretical simulations described in section IV.A.1 indicates that strong interaction forces can distort the interface into commensurate contact[153,156] and produce periodic lateral forces.

These observations raise the issue of commensurability. If two contacting surfaces possess no preferred relative position, there should be no resistance to relative sliding, analogous to the transport of an incommensurate charge density wave in a solid.[199] Defects and deformation obviously complicate the situation. These ideas have been pursued theoretically.[26,156,162,163,200] Hirano *et al.*[201] showed that frictional forces between mica sheets in contact in a SFA experiment were maximal when the orientation of the mica sheets matched. Friction forces were a factor of 4 lower when the crystallographic directions of mica sheets were misoriented relative to each other. Although Hirano *et al.* have claimed to have proven the existence of "superlubricity" (absolute zero friction), actual confirmation of absolute zero friction remains to be made. It would be very interesting if more experimental work can be performed to further explore this point.

We point out that the study of grain boundaries in materials is another example of interfacial phenomena which depend upon atomic structure and orientation. We refer the reader to Sutton and Balluffi's wide-ranging text[202] and references therein. This is a well-established field with many overlapping topics with nanotribology, including the study of friction. We encourage further consideration of the links between these fields.

4. Chemical Effects

Along with atomic orientation, the role that the chemical environment and the chemical identity of species at an interface play in determining friction is not fully understood, and FFM measurements can address this. The sensitivity of lateral forces to chemical identity can also be exploited to achieve surface chemical imaging. This area of research with FFM is relatively new. Marti *et al.*[203] have shown that changes in pH can affect friction. They measured lateral forces between a silicon nitride tip and a flat SiO_2 sample immersed in solution. Varying the pH changed the amount of protonation of OH groups on the tip and sample surface, thus changing the amount of surface charge, depending on the isoelectric points of the tip and sample materials. This affected the interaction forces between tip and sample and the resultant dependence of friction upon load varied with pH. With this technique, materials with different isoelectric points should produce contrast in FFM images, depending on the pH of the surrounding solution. The authors also attempt to correlate the observed friction with adhesion hysteresis. Adhesion hysteresis refers to variations of adhesion with contact time or with displacement direction (advancing *vs* retracting) and has been observed with the SFA.[166,178] It must be distinguished from the simple mechanical hysteresis which occurs for a compliant lever contacting a surface (snap-in *vs* pull-off, see Figure 1b). Adhesion hysteresis can occur when complex varying processes at the interface take place, such as interdigitation of surface molecules, which change the interfacial adhesion energy and that recover over time scales that are longer than the measurement time. Since the adhesion energy affects the contact area, observing different contact areas (or different values of friction) at the same load during advancing *vs* retracting would be a clear indication of adhesion hysteresis. It is not clear that this has been observed in the FFM experiments of Marti *et al.* described above, but this possibility is worthy of further pursuit since it would be indicative of a specific contribution to frictional dissipation, provided that the exact mechanism of the hysteresis (mechanical, chemical, *etc.*) can be identified.

Binggeli *et al.*[204] studied changes in frictional forces under varying electrochemical conditions. They measured frictional forces between the FFM tip and a graphite surface in an electrolytic solution as a function of the sample potential. They found that there was an electrochemical dependence of the

frictional force at graphite step edges. In a certain sample potential range, friction was strongly enhanced at step edges. This is similar to effects previously mentioned in section IV.A.2 for steps on the NaCl surface in a dry nitrogen environment.[173] Clearly, the increased surface energy at steps is contributing to increased friction. Further experiments on more materials in different environments should help to explain this behavior.

Other aspects such as the effect of humidity on tip−sample forces have been discussed by Binggeli and Mate,[205] Hu *et al.*,[102] and Schumacher *et al.*[206] Further examples where the chemical identity of monolayer films are varied and measured in FFM experiments are discussed in section V.

B. Wear and Plastic Deformation

1. AFM Measurements

So far we have discussed friction measurements in the elastic regime, below the load threshold for observable damage to take place. However, plastic deformation is an irreversible form of work, *i.e.*, energy dissipation, and thus can be important in determining the frictional behavior of real materials in contact, although a comprehensive atomic-scale understanding of this relationship does not yet exist. Furthermore, substantial amounts of plastic deformation and wear are often present in real sliding contacts[207] and therefore understanding the causes of wear and how to reduce it are obviously of great practical importance. As mentioned in section IV.A.2, the properties of the contact between regular materials are determined by very small asperities whose mechanical properties may differ substantially from bulk properties. Force microscopy and related techniques have begun to address atomic-scale tribological phenomena such as plastic deformation and wear. While several investigations of wear have been carried out using AFM,[208−211] here we will focus on atomic-scale studies.

As discussed in section I, contact mode AFM lacks the resolution to image individual point defects, and so it is not yet known whether or not low-load scanning actually creates point defects in materials. Such effects have been predicted by theoretical modeling by Shluger et al.[157] Their study showed that lateral forces with the periodicity of the atomic lattice can occur between an inert MgO tip and the cleavage surfaces of NaCl and LiF, and a tip with a chemically active OH^- group on its end produced point defects in the sample even at low loads. These defects included formation of vacancies and interstitials in the sample surface, and individual ion motion from the sample to the tip. Lattice periodicity was not obtained under these conditions, and friction forces were higher. Further simulations demonstrating atomic-scale wear of tip and sample have been performed by Landman *et al.*[159,160,165] and Sørensen *et al.*[156] These studies suggest that imaging conditions can be greatly affected by tip and sample composition, and that such processes can be important in determining friction. These effects should therefore be considered. The newly developed noncontact force-modulation mode with AFM[98] can image point defects, and perhaps this technique could be used to image the exact atom-by-atom effect that tip contact has on a surface.

If indeed atomic defects are produced during sliding which either anneal away or simply are not observed due to lack of true atomic resolution, then this should contribute somehow to the friction force. The nature of this contribution has not yet been modeled and is worthy of serious consideration.

Several AFM experiments have observed nanometer-scale tip-induced wear of the sample[70,102,118,188,212−220 164] and even wear of the tip itself.[221,222] Theoretical predictions for wear of both sample or tip[156,157,165,223−225] have also been performed. Several of these have shown that observable wear (as imaged afterward by the AFM tip) can occur on a surface by sliding the tip in contact above some threshold load, below which no damage is observed. This type of behavior has been reported with various materials including Si(100), Mn−Zn ferrite (used in hard disk slider heads) and a Au film,[215] SiO_2,[212,214] AgBr and C_{60} islands on NaCl(100) in UHV,[70] KBr-(100) in UHV,[164] lead pyrophosphate ($Pb_2P_2O_7$),[226] MoS_2 and $NbSe_2$,[227] $NaNO_3$,[220,215] and muscovite mica.[102,218,219] Some of these studies monitored frictional forces while increasing the load and generally observed sudden or anomalous increases in friction when extensive wear started to occur, indicating that shear processes cause the wear. The example of mica from Hu *et al.*[102] is shown in Figure 15a. In this case, the layered structure of mica allowed a single atomic layer, 1 nm deep, to be removed by the tip, an observation made both by Hu *et al.*[102] and Miyake[218,219] (Figure 15b). The atomic layer could be removed by single scans at high loads, or multiple scans at low loads. The latter observation provides another hint that atomic-scale defects can be produced (although not observed) in the low-load regime. The sudden appearance of substantial wear after repeated low-load scans led Hu *et al.* to suggest that point defects were accumulating during the low-load scanning. Miyake showed that single or multiple layers could be controllably removed in a "processing" fashion. The newly exposed layer is atomically smooth. Unfortunately, the tip radius in these experiments was unknown and so the critical pressures required for these processes are as yet undetermined.

A layered material of great tribological interest is MoS_2, which is used as a solid lubricant.[228−230] MoS_2, like other transition metal dichalcogenides, forms layers which are weakly bonded together by the van der Waals interaction. Kim *et al.*[227] performed a comparative study on MoS_2 and another layered material, $NbSe_2$, and observed that atomic layer-by-layer wear could be induced by the tip and that this wear occurred more readily on $NbSe_2$. Furthermore, the boundaries of nanometer-scale wear regions on $NbSe_2$ corresponded to the tip scanning directions, whereas wear region boundaries on MoS_2 corresponded to crystallographic directions. This suggests that, compared to $NbSe_2$, the MoS_2 surface possesses greater intrinsic stability and this may help to explain its superior lubricating properties.

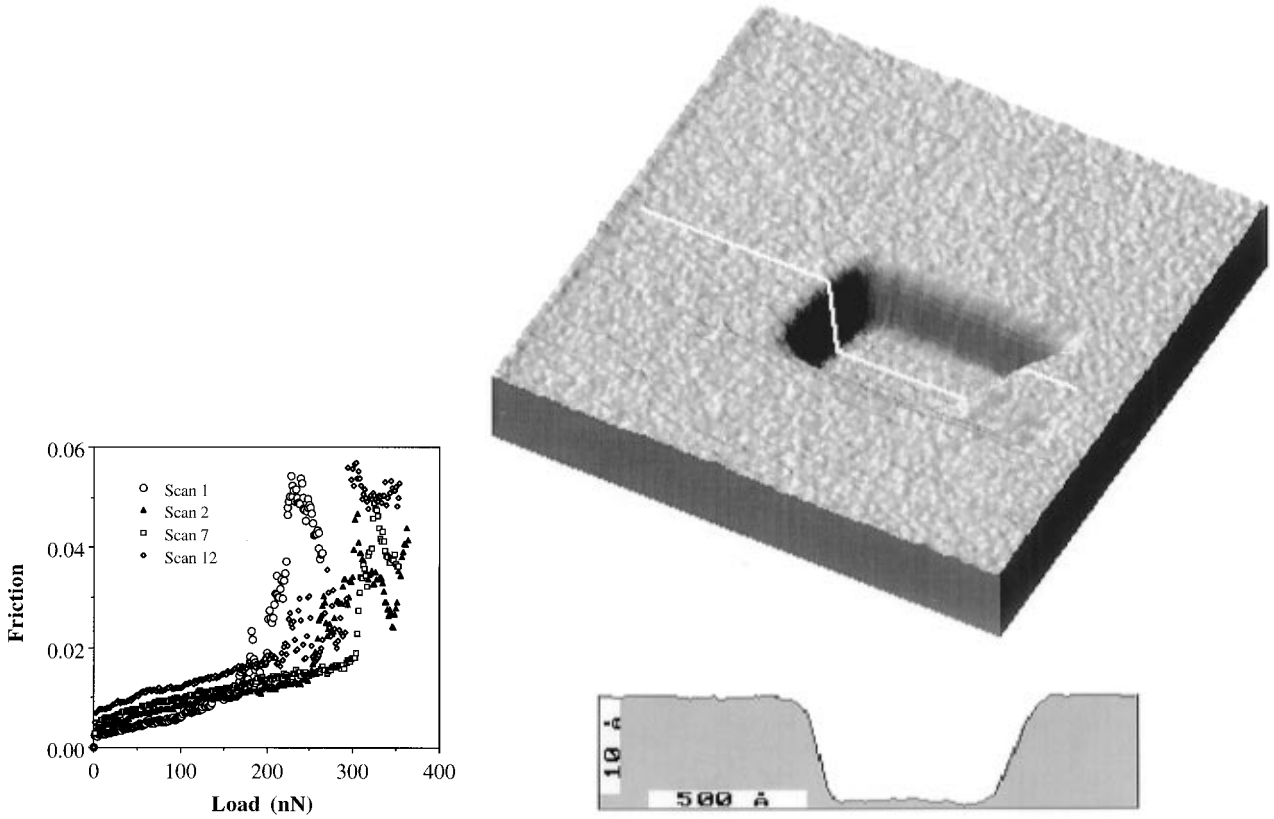

Figure 15. (a, left) Friction force (au) *vs* load in the high-load regime for multiple scans of a silicon nitride tip in contact with mica. Friction increases smoothly with load until wear occurs, where substantial peaks are seen. (b, right) A 150 × 150 nm image showing wear of mica. The hole is 1 nm deep, corresponding to one atomic layer of mica. (From Hu *et al.*[102] Copyright 1995 Elsevier Science B.V.)

Lüthi *et al.*,[188] in an experiment with C_{60} islands grown on NaCl(100) in UHV, were able to fracture a C_{60} island with the tip and thus determine the energy needed to separate the C_{60}'s. The measured cohesive energy of 1.5 ± 0.3 eV per C_{60} molecule was similar to other theoretical and experimental values. This shows that with AFM, quantitative measurement of pressure- and shear-induced modification can be examined.

Real-life wear process are often influenced by the chemical environment. An example of "tribochemical wear" was investigated with AFM on a model material by Nakahara *et al.*,[220] where the surface of $NaNO_3$, a hygroscopic salt crystal, was subjected to wear from the combined effect of humidity and tip contact. Using a silicon nitride tip on the cleaved sample, wear began at defect sites. Degradation of cleavage steps was induced by contact scanning with the humidity >45%. Diatomic steps were seen to split into monatomic steps and material was dragged from steps to the terrace above. With repeated scanning, nanometer-sized rows of material could be piled up in a roughly periodic fashion on flat terraces. Essentially, tip contact was promoting sample dissolution. Humidity-dependent atomic layer-by-layer wear was observed by Thundat *et al.* on lead pyrophosphate ($Pb_2P_2O_7$),[226] which was induced by scanning at humidities >25%. In this case, increased capillary forces at higher humidities leading to greater mechanical interaction between tip and sample was suggested as the wear mechanism, as opposed to sample dissolution. Systematic studies such as these, with materials in various environments, could lead to an understanding of the interplay between chemical environment and sliding contact conditions in determining certain wear processes.

The force-controlled experimental methods described in section II.D.4 allow simultaneous measurement of the indentation depth and the applied force, and so they are useful for investigating plastic deformation. A polycrystalline Au film was studied with this technique by Thomas *et al.*[231] The film was prepared by thermal evaporation and then coated with 1-octadecanethiols to form a passivating self-assembled monolayer that reduced tip−sample adhesion (further details of the mechanical properties of such monolayers are described below in section V). The Au film consisted of many grains of tens to hundreds of nanometers in diameter. Measurements were carried out with tip and sample immersed in hexadecane to avoid capillary forces. They found that when a 250 nm radius W tip made contact with a protruding grain in the passivated Au film, there was an initial elastic response described by the Hertzian model. As the load is increased, the entire nanometer-size gold grain plastically yielded, being pushed downward relative to the neighboring grains, filling some subsurface free volume. Grain boundary slippage is thus identified as the initial mechanism of plastic deformation. At yet higher loads, no more subsurface free volume remains and the grain itself begins to plastically yield with a measured shear stress threshold for plastic deformation of 2.6 GPa, much higher than the value for bulk Au of ~200 MPa, but of the order of the ideal theoretical yield stress for Au in the absence of dislocations of ~1.5 GPa.[232,233]

Similar AFM measurements by Salmeron *et al.*[234] on Au surfaces with Pt−Rh tips produced hardness values of 1 ± 0.5 GPa, which also corresponds to a yield stress significantly higher than the bulk value. These experiments also showed that dislocations can be created near the indented area. Sutton and Pethica[235] also observed near ideal yield stress values using diamond tips indenting W surfaces. More experimental observations of nm-size contacts with strengths far above the bulk value will be discussed below. Measurements such as those described here are important because they allow quantitative determination of the yield processes of important materials such as thin films, and also provide insight into the details of deformation behavior at the nanometer-scale.

2. Atomic-Scale Metallic Contacts

Very exciting results have been obtained by simultaneously measuring the force and electrical current in a nanometer-sized metallic contact under stress by Agraït and co-workers[236,237] and Dürig and Stalder.[238−240] In these experiments, a tip and sample of the same material are brought into contact to form a nanometer-sized single asperity contact. The applied load is measured by cantilever deflection[236,237] or an oscillating force sensor.[241] In either case, nanonewton force sensitivity is achieved. A small bias voltage (∼10 mV) is applied and the current through the contact is measured. In this size regime, the contact is smaller than the mean free path of the electrons, and the conductance, in the absence of interchannel mixing, is essentially given by the Landauer−Büttikker formula[242]

$$G_c = G_0 \sum_{j=1}^{N} T_j \qquad (8)$$

where G_0 is the conductance quantum $2e^2/h$, T_j is the transmission probability for the jth electron conduction channel, and N is the total number of conduction channels, which is determined by the geometry of the contact. N can be shown to be proportional to the area of contact, and T_j can be shown to be close to 1 for each channel, thus the conductance is proportional to the contact area. For an exact description of atomic-size contacts, this simple formula must be modified as the exact structure of the contact becomes important.[243] In general, discrete changes in the conductance of the contact are expected if atomic rearrangments of the contact occur. An example of such measurements from Agraït and co-workers[236] is shown in Figure 16. The inset in Figure 16a shows the set up; the contact is formed between the gold tip and a gold sample substrate. The gold sample is mounted on a stiff cantilever that deflects in response to forces between the tip and sample. The experiment was carried out at room temperature in ambient atmosphere. Figure 16a shows the conductance as the tip is pulled back from the sample after a contact had already been formed. Figure 16b shows the corresponding force. Starting from the right-hand side of the figure, as the tip is pulled back from the sample, the tensile force increases with constant slope (*i.e.*, elastically),

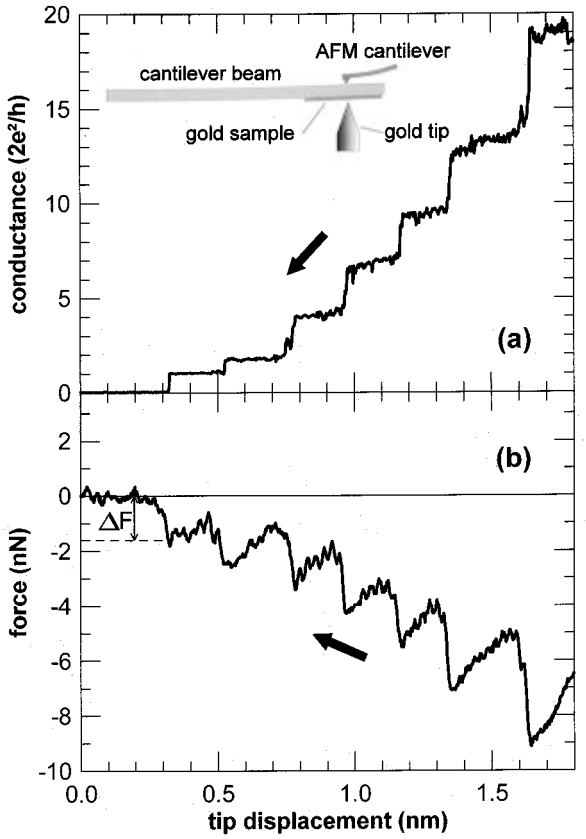

Figure 16. Simultaneously acquired (a) conductance and (b) force measurements during the elongation of gold connective neck (the tip displacement occurs from right to left). Each drop in conductance occurs in nearly integral numbers of the conductance quantum ($2e^2/h$) and corresponds exactly to a relaxation of tensile force. The final force relaxation $\Delta F = 1.5 \pm 0.2$ nN. The inset to a describes the experimental setup. Deflection of the AFM cantilever is used to determine the force exerted by the gold tip on the gold substrate. (Reproduced with permission from Rubio *et al.*[236] Copyright 1996 American Physical Society.)

then suddenly relaxes. At exactly this point, the conductance exhibits a sudden decrease. This behavior continues until the tip is pulled out of contact with the sample. The conductance is seen to change in a stepwise fashion and each step is associated with a relaxation in the tensile force. Conductance steps during pulling metallic contacts have been observed by other groups with STM techniques.[244−246] The behavior can be explained as a sequence of structural transitions of the contact involving elastic and yielding stages. Each force/conductance jump is associated with an atomic rearrangement of the contact which relieves the tensile stress and changes the number of conduction channels present. Similar observations in vacuum were made at 4.2 K[237] and at room temperature.[238−240] The observations are in agreement with molecular dynamics simulations.[225,247,248] Notice that the very last relaxation before the contact is broken involves a single conductance quantum and a force jump of 1.5 ± 0.2 nN. This is precisely the force and conductance change expected for the breaking of a single atom contact.[249] Since forces and contact areas can be determined, the apparent pressure at which the contact yields plastically can also be determined. This pressure ranges from 3 to 6 GPa for contact areas >1.2 nm^2, more than 20 times the value for a macroscopic contact and

3−6 times higher than that determined with previous AFM experiments[117,231−234,250] which involve contact areas of several hundred nanometer^2. The result agrees with Stalder and Dürig's value of 6 GPa for the yield stress also for a gold nanocontact.[238−240] At smaller contact sizes, the yield pressure is even higher, rising to 13 GPa for the last yield point. This is also in agreement with MD predictions.[122,247,251] Evidently, the contact is small and ordered enough that dislocation motions are not determining the plastic behavior. Agraït's experiments also showed that, for all but the smallest contacts, the elastic stiffness of the contact is comparable to predictions of continuum elastic theory. These remarkable observations at room temperature indicate that dramatic *atomic-scale* phenomena can in fact be observed, and are in fact important if all the processes involved in regular sliding contacts are to be understood.

V. Model Lubricated Interfaces

In this section we will focus on applications of AFM to studies of model lubricants, in the form of self-assembled (SAM) or Langmuir−Blodgett (LB) monolayers. Because they form densely packed and often ordered structures on solid surfaces, they are ideal to model lubricant films for fundamental studies of tribology. The advances in this field using AFM have been spectacular in recent years. We will not consider in this review the vast number of AFM studies that have been devoted to determine the ordered structure of many monolayers, their stacking on surfaces, and such important properties as phase segregation of multicomponent systems, nanoscale manipulation, studies of biological material, polymers, *etc.* Instead, we will limit our review to a few topics, including the intercorrelation between friction and molecular structure, elastic and adhesive properties, and finally and more extensively, on the molecular structure of the organic layers when subjected to uniaxial compression.

Because of the large number of properties that can be designed into SAM and LB films, they offer almost unlimited possibilities for studies to correlate many surface and film parameters with friction and adhesion. For example, the binding to the substrate can be changed by using molecules with different head groups: −SH (thiols), −SiR_3 (silanes), −COOH (acids), *etc.* The softness or elastic compliance can also be changed by modifying the chain length and/or the type of chemical bonds inside the chains (single, double, and triple C−C bonds), by fluorination, and by inclusion of several heteroatoms, like O (in ethers), *etc.* All of these modify the rigidity of the chains. The end groups that are exposed to the vacuum or liquid interface can also be conveniently modified to affect the friction and adhesion forces.

In order to review the present status of knowledge of the molecular structure of model lubricants under shear and compressive forces, we will summarize first what is known about the structure under zero applied forces. We will then focus on the structure under compression in various pressure regimes. For these studies it will be necessary to combine the AFM (and its cousin, the SFA) with other spectroscopies, such as the nonlinear optical techniques of second-harmonic generation (SHG) and sum frequency generation (SFG) that can selectively access buried interfaces with monolayer sensitivity.

A. The Structure of SAM and LB Films

Under zero external load, the film molecules exchange energy mostly by thermal processes. The short- and long-range structure of the monolayer is determined by intermolecular and substrate−film forces. The relative strength of these two interactions determine both the degree of order and the epitaxial relationship with the substrate. It is therefore useful to consider typical energy values for these interactions. In the common case of normal alkane chains, the van der Waals energy per CH_2 group in a close packed arrangement of straight, parallel chains at their crystalline separation of ∼4.5 Å, is ∼7 kJ/mol, provided that the chain length is above ∼6−8 carbon atoms long.[123] This gives a total van der Waals energy of a C_{18} alkane of about 126 kJ/mol, which is comparable to the energy of a covalent bond, in the range of 100−300 kJ/mol. Thus we can predict that for short chains thiols (C_n, $n < 10$), the molecule−substrate interaction is the dominating force, while for $n > 12$, chain−chain interactions play a determinant role. A study by Butt *et al.*[252] seems to confirm these ideas. These authors used polycrystalline Au substrates and found that closed packed hexagonal structures are formed by C_{18} thiols even in areas of the sample where the Au substrate is disordered, or at least not of (111) orientation. This indicates that for these chain lengths, the chain−chain interaction is the dominating force for the ordering of the long chain thiols. For alkylsilanes, covalent bonding between the chain heads, in addition to head−substrate bonding, will be a dominant interaction.[253] The following is a summary of the structure of SAM of alkyl chains with −SH (thiols) and −SiR_3 (silanes).

1. Thiols

Ordered monolayers of thiols on Au(111) have been widely used since they were discovered by Nuzzo and Allara 14 years ago.[254] They have been studied by a variety of techniques that suggest dense packing of the chains and an absence of gauche defects.[254−256] Diffraction studies using electrons,[257] He scattering,[258] and X-rays[259] have firmly established the crystalline structure of the thiol monolayers, which consists of a basic $(\sqrt{3}\times\sqrt{3})R30°$ periodicity relative to the Au(111) lattice with a superstructure of $c(4\times2)$ times the basic $\sqrt{3}$ structure. The nature of the larger periodicity was not uncovered until recently by Fenter *et al.*[260] using X-ray diffraction. These studies have revealed the formation of S−S bonds at the metal interface, which indicates that not all the S atoms occupy the 3-fold hollow sites of the Au substrate as assumed initially. This has been confirmed by another recent study using SFG.[261]

A tilt of the molecular axis to about 30° from the normal is also observed and has been explained as a result of a space-filling configuration to maximize the van der Waals energy. This explanation is based on the molecular diameter of 4.5 Å, which is smaller

than the $\sqrt{3}\, a_{Au}$ (= 5 Å) distance of the Au substrate. Other contributions to the tilt can be important, for example, the matching, or in-phase locking, of C−C−C angles in adjacent chains.

The application of STM to determine the SAM structures deserves special comment since the insulating nature of the alkyl chains imposes operation at very high tunneling gaps, a condition that was not realized in many earlier studies.[262,263] Operation at high gaps is necessary to ensure the presence of a true vacuum gap, *i.e.*, to avoid contact, between the tip and the CH_3 terminated surface (see U. Dürig *et al.*[264]). While this is easily feasible for short length chains (<10 carbons), it becomes difficult for the longer chains due to the rapidly decreasing tunneling probability. Calculations of the tunneling probability as a function of chain length[265] show that only for lengths <10 carbon atoms is the tunnel current in a range that is within typical values of the preamplifiers used in STM. Under these conditions, ordered structures were observed by Poirier *et al.*[266] and by Anselmetti *et al.*[267] that agree with the He scattering and X-ray diffraction results, indicating that STM is a valuable technique in studies of model lubricant layers.

The calculations[265] also predict that nonlinear increases of the tunneling current will occur during compression of the molecular layer, leading to an increase of the tilt angle. It would be very interesting to further pursue this line of research by determining both theoretically and experimentally the tunneling current changes due to increased distortions of the molecular structure (inclination of the chain axis, formation of gauche defects, *etc.*).

Fluorinated alkanethiols have also been studied. The diameter of the $-CF_2-$ chains (5.76 Å) is larger than the $\sqrt{3}\, a_{Au}$ (5 Å) distance, and closer to $2a_{Au}$ (5.8 Å). Indeed, a hexagonal structure with 5.8 Å periodicity is formed. However, the structure is *incommensurate* with the substrate by a 30° rotation.[268] So it appears the S ends prefer again to bind to sites other than the 3-fold hollow sites which are usually the lower energy sites for S atoms adsorbing in hexagonal close packed surfaces. This is another example of the dominant role played by interchain van der Waals forces in long molecules.

2. Silanes

Alkylsiloxanes constitute another widely used class of self-assembling molecules. The active end group is SiR_3, where R usually stands for chlorine, ethoxy (OCH_2CH_3) and other groups. These molecules also form compact and strongly bound monolayers on oxide substrates, notably SiO_2, in quartz and glass that contain surface hydroxyl groups. Reviews on their structure and preparation can be found in the literature.[269] Besides many common characteristics with the alkanethiols, which derive from the similarity between the van der Waals chain interactions, the SAMs formed by the alkylsiloxanes exhibit some notable differences. The most important one is the covalent bonding between molecules by formation of siloxane bridges, Si−O−Si, linking adjacent molecules. This cross linking is absent in the case of thiols. Since the length of the siloxane bridge is 2.6 Å, while the alkane chain diameter is 4.5 Å, distortions at the head groups near the substrate are inevitable. Thus, while it has been established that the monolayer films are molecularly flat,[253] and have a thickness in agreement with their chain lengths,[270−273] no long-range order has been detected by any of the aforementioned techniques. The importance of the intermolecular cross-linkage in stabilizing the film, particularly on mica, where no substrate OH groups are present, was demonstrated by a recent study by Xiao *et al.*,[253] using mono- and trisiloxane head groups. The former ones cannot form bonds to neighboring molecules and were found to form unstable films.

B. Friction, Adhesion, and Chemical Identity

Meyer *et al.* demonstrated from the early stages of application of FFM that friction is clearly dependent on the chemical identity of the exposed end groups and that this can be used to identify the surface films. In their study[274] the friction contrast of the exposed AgBr substrate was higher than that of the Cd−arachidate LB films, while no difference was observed between different layers of the film. Similar results were obtained with Cd−arachidate films on Si.[190] Mixed films of long chains of normal and fluorinated acids were studied with FFM by the same group. Segregation into separate phases could be observed by the topographic images and confirmed by the simultaneously acquired friction images. Lower friction (by a factor of 4) occurred on top of the normal hydrocarbon domains.[99,275]

More recently, the connection between chemical nature, adhesion and friction has been established by Frisbie *et al.*,[100] who demonstrated different adhesion between surfaces (tip and substrate) coated with molecules exposing a variety of end groups: CH_3/CH_3, CH_3/COOH, and COOH/COOH. The adhesive forces were found to be in the order COOH/COOH > CH_3/CH_3 > COOH/CH_3 with the corresponding frictional forces following the exact same order. Another study along the same lines was conducted by Green *et al.*,[276] who demonstrated similar effects with a large number of functional groups at the end of molecules of similar length (15 carbon atoms) attached to one or both surfaces (CO_2H, CH_2OH, CO_2CH_3, CH_2Br, CH_3 terminations). Interestingly, the frictional forces ranked in the same order given above and show a clear correlation with the surface energy as measured by macroscopic methods such as water contact angle. These results are shown in Table 2. These findings follow the intuitive idea that both adhesion and friction are expected to be larger on high surface energy materials.

C. Friction, Adhesion, and Elastic Properties

Another interesting correlation has been established by Overney and co-workers between friction and the elastic properties of the films.[105,277,278] The force modulation technique described in section II.D.3 was used to measure the elastic compliance of the system. The authors applied this technique to study the segregation of mixtures of normal and fluorinated molecules forming LB films transferred onto Si(100)

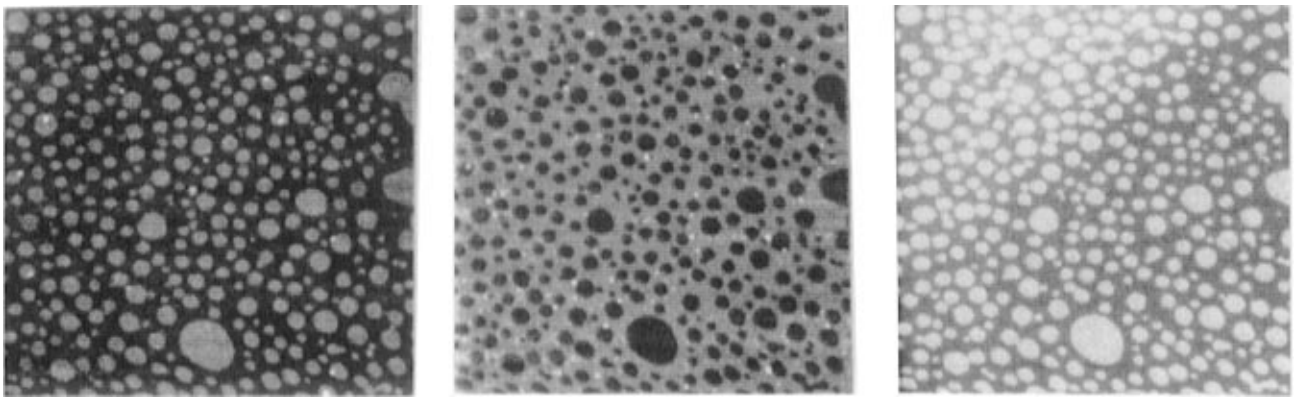

Figure 17. Simultaneous AFM measurement ($3 \times 3\ \mu m^2$) of topography, friction, and elasticity of a monolayer film of a 1:1 molar mixture of BA and PFECA prepared at pH 6.6. (a, left) Topography with island-like hydrocarbon domains of ~80 nm in diameter on top of a sea-like fluorocarbon film. Gray scale: dark = low, bright = high. (b, middle) Friction force map shows lower friction (dark) on hydrocarbon islands and three times higher friction (bright) on fluorocarbon sea. Friction on fluorocarbons is measured to be 12.6 ± 2 nN. (c, right) Elasticity map shows higher Young's modulus (brighter) on the hydrocarbon domains. The relative difference in elasticity is 0.1 ± 0.03 GPa. (Reproduced with permission from Overney *et al.*[277] Copyright 1994 American Chemical Society.)

Table 2. Frictional Parameters for the Contacts Formed between an Uncoated Silicon Nitride AFM Tip and Several Different End-Group Terminated Alkanethiolate Monolayers ($Au-S(CH_2)_n-X$) Chemisorbed on Au(111)[a] (Reproduced with permission from Green *et al.*[276] Copyright 1995 American Chemical Society.)

end group[b]	$\cos\theta_a$[c]	α	f_0 (nN)	f (nN) for $F_N = 20$ nN
CO_2H ($n = 15$)	~1	0.76	22	42 ± 7
CH_2OH ($n = 15$)	~1	0.70	8	40 ± 6
CO_2CH_3 ($n = 15$)	0.39	0.34	10	20 ± 5
CH_2Br ($n = 20$)	0.12	0.26	~0	9.4 ± 2
CH_3 ($n = 17$)	−0.37	0.070	~0	1.4 ± 1

[a] Values of α and f_0 are respectively the slopes and y intercepts obtained from linear least-squares fits of friction *vs* load data. [b] n equals the number of methylene groups in the polymethylene chains. [c] This column correlates the surface free energies of the different monolayers with the advancing contact angle (θ_a) of water as a probe liquid. Thus through the Young relation, the larger $\cos\theta_a$, the greater the surface free energy.

substrates. They obtained simultaneous maps of elastic compliance, friction, and topography. The fluorocarbon component was observed to form a flat film in contact with the substrate while the normal hydrocarbons ($C_{21}H_{43}COO-$) formed islands on top of the fluorocarbons. The images in Figure 17 show that the topographically higher and stiffer hydrocarbon component also show lower friction. These results translate concepts proven valid in more macroscopic experiments (see, *e.g.*, Bowden and Tabor[15,16]) to the nanometer scale. Thus, the softer component will give rise to a larger contact area for equivalent loads, which in turn leads to a higher frictional force.

Another combination of scanning modes on segregated films of 17 and 25 carbon long alkyl chain organic acids was performed by Koleske *et al.*[279] These authors obtained simultaneous images of topography, adhesion (or, more appropriately, pull-off force), and friction. They showed that high friction is associated with high adhesion. The study is interesting because here the end groups of the two types of domains are identical (CH_3). The authors established that the higher adhesion observed in the C_{16} domains is due to the higher compliance of the shorter chains, again a manifestation of the larger contact area in the softer component. Together with the previous results, a common line can be observed in all the phenomena: high friction is associated with high adhesion and/or high compliance, although the last two are not necessarily related. Compliance is a property of the entire molecule and of the structure and packing of the chains together on the substrate. In a study by Xiao *et al.*,[280] the friction of a SAM of alkylsilanes on mica was found to be a strong function of the alkyl chain length, with the shorter chains exhibiting the highest friction. These results are important because they separate the effects due to the chemical nature of the end group, CH_3 in this case for all the chains, from other contributions. The higher friction was interpreted as due to the poor packing of the shorter molecules, which in turn is a result of the decreased van der Waals interchain forces, as discussed in the previous section. The poor packing gives rise to more energy dissipating modes (chain bending and tilting, rotations, formation of gauche defects, *etc.*), which can be excited during frictional sliding. These modes are stearically quenched in the densely packed films formed by the longer chain molecules. A more recent study by Lio *et al.*,[281] extends these results to thiol films on gold and presents a detailed comparison with the friction of silanes of the same length. While for C_{18} chains, both thiols and silanes show very similar frictional forces, for shorter chains the friction force is higher on silanes and the difference increases as the chain gets shorter, down to C_6. The study demonstrates that *short*-range order and packing being similar, as in the case of the longer C_{18}'s, the friction is also similar, while as the packing decreases in the silanes relative to the thiols for the shorter chains, the friction increases.

D. Molecular Structure of Films Under Moderate Pressure (<100 MPa)

Using SFG, spectroscopic studies of the effect of pressure, in the range from 10 to 100 MPa, were performed by Du *et al.*, using a simple SFA consisting of a flat and a sphere.[282] With spheres of centimeter

radius, contact diameters ranging from micrometers to millimeters were generated by elastic deformation of the substrate materials, with average pressures of 10 to 100 MPa. While in principle one can utilize many molecular-specific optical spectroscopies, such as absorption, fluorescence, IR, and Raman, their selectivity to the buried interface is low. The nonlinear optical techniques, specifically SHG and SFG, are free of this problem by virtue of the inversion symmetry selection rule, which eliminates the contribution from bulk processes in centrosymmetric materials from the observed signal.

The authors performed experiments using LB films of stearic acid, alcohols and covalently bound self-assembled monolayers of octadecyltriethoxysilane (OTE). The main feature of the SFG spectrum is the stretch mode of the methyl groups at 2875 cm^{-1}. The resonance corresponding to the CH_2 groups in the middle of the chains, at 2820 cm^{-1}, is absent in the spectrum. These observations are the result of the selection rule mentioned. Only the terminal CH_3 groups lack inversion symmetry, while the CH_2 groups are arranged in an alternating fashion along the chain, with inversion symmetry points in the center of the C−C bonds. The absence of the CH_2 stretch indicates that the molecules are straight, *i.e.*, in an all-trans configuration. Only when kinks are formed in the chains is the inversion symmetry broken and the CH_2 stretches might be observable. This is indeed observed in uncompressed films of fatty acid on the surface of water, where the poor packing makes possible the presence of many thermally activated kinks.[283] After pressing the two surfaces together, with a monolayer adsorbed on one side only, in all cases the SFG spectra showed a strong decrease of the CH_3 signal intensity below the noise level, indicating that the second-order nonlinear susceptibility decreased by at least 2 orders of magnitude. This occurred as soon as the area of contact contained the entire laser beam spot, at a pressure of 10−20 MPa. No intensity in the CH_2 stretch region was observed above the noise level. The vanishing of the SFG signal was completely reversible and, upon separation of the surfaces, the shape and intensity of the spectrum was completely recovered. Similar observations were made with the OH stretch mode, at ∼3500 cm^{-1}, in the case of alcohols and acids. When the contact diameter increased to a value of ∼1 mm, the intensity of the CH_3 and OH stretch modes was measured as the laser beam was scanned across it (Figure 18). The signal oscillations outside the contact region are due to multiple interference effects, from reflections between the lens surfaces, as the gap increases away from the contact zone. In the case of the C_{18} silane, at 20 MPa the CH_3 stretch mode decreased to ∼10% of its original value at the center (where the pressure is maximum) and somewhat higher near the edges. Raising the pressure further to 80 MPa caused the extinction of the CH_3 stretch signal over the entire contact area, and the cross-sectional scans were similar to those shown in Figure 18. The absence of the CH_2 stretch intensity persisted up to 0.2 GPa, the highest pressure reached. The vanishing of the nonlinear second-order susceptibility was interpreted

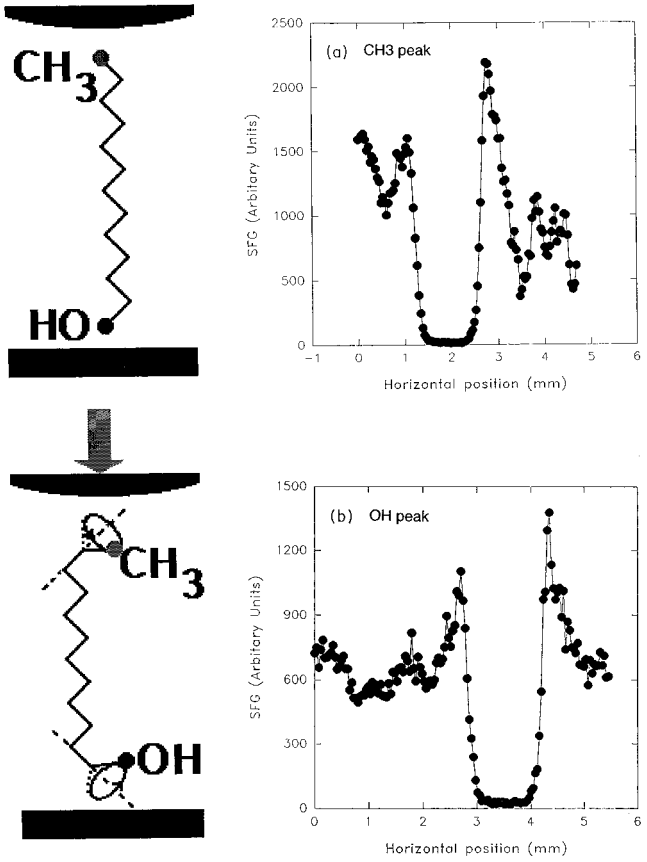

Figure 18. SFG signal intensity of the CH_3 symmetric stretch mode (a) and OH stretch mode (b) of an octadecyl alcohol Langmuir−Blodgett monolayer on a flat fused-quartz *vs* laser spot position in the contact area. Inside the contact, the SFG signal decreases by a factor of 1000 into the noise level. Oscillations in the outer region are due to multiple interferences of the beam. The average pressure is ∼50 MPa. The schematic drawings on the left illustrate the geometry of the molecule before (top) and after (bottom) compression. (From Du *et al.*[282] Copyright 1995 The American Physical Society.)

as follows: under pressure, gauche distortions are created at the free end of the molecules (the CH_3 and OH ends for the LB alcohols and the CH_3 end for the silanes) that bring the dipole moments of the CH_3 and OH groups to a nearly parallel direction to the surface (see schematics in Figure 18). In addition, the direction of the CH_3 dipole in the surface plane is random, from one molecule to the next, producing a random phase addition of their radiation fields; hence the vanishing of the SFG signal. The remainder of the alkane chain (the central part) remains undistorted *i.e.*, straight, as shown by the nonappearance of the CH_2 stretch intensity. Since a simple end gauche distortion would produce a nonsymmetric CH_2 group while no CH_2 stretch mode is observed in the SFG spectrum, one must assume that the dipole moments of this mode are also randomly distributed. These might indicate additional gauche distortions in the few next CH_2 groups. The combined effect would be a small vertical compression of the chains of a few angstroms. These results are in line with the findings of Monte Carlo simulations by Siepman *et al.*,[284] who concluded that the gauche defects are essentially concentrated near the molecular ends.

E. Molecular Structure of Films Under High Pressure (>1 GPa)

At the sharp asperities that mediate the contact between solid surfaces and in AFM experiments, the pressures can easily reach values close to and above several gigapascals. In view of the findings presented above, this implies that, under typical AFM imaging conditions, self-assembled and L−B films of organic molecules are always distorted under the tip with gauche defects at the terminal chain groups. The fact that the thiol $(\sqrt{3}\times\sqrt{3})$R30° periodicity on Au(111) is still observed is remarkable. It indicates that, under the near GPa pressures, the average distance between chains is maintained, in spite of the existence of gauche defects at the end groups discussed in the previous section. This is a consequence of the large contact area under the load applied. For example, for a 200 Å radius tip and a load of 5 nN, the Hertzian contact diameter for Au is estimated to be ∼15 Å and thus to include ∼35 thiol molecules. The c(2 × 4) superstructure observed by diffraction techniques and by STM at zero pressure is lost in the AFM images since it implies order of the C backbone planes, which can only be present in the absence of gauche deformations. We will now examine the effect of pressure on the structure and packing of the SAM monolayers. Since, as we will see, the effects depend strongly on the tip radius in addition to pressure, we will examine examples that represent two extremes of this dependence.

1. Large Tip Radii (R > 1000 Å)

The response of self-assembled alkanethiol films on gold was studied by Joyce *et al.*[285] using a force-controlled AFM, as described in section II.D.4. They used ∼5000 Å radius W tips and forces in the micronewton range which produced pressures of a few gigapascals. They found that the thiols could be viscoelastically compressed, with slow recovery times on the order of 0.08 s, which, according to the authors, is indicative of pressure-induced chain entanglement.

Along the same lines, the response of thiol monolayers of 12- and 22-carbon long alkane chains on Au(111) to pressure by Pt−Rh tips of 1000−3000 Å radius has been studied by Salmeron *et al.*, using ac force modulation techniques at frequencies close to the mechanical resonance of the supporting cantilevers.[265,286] The cushioning effect of the thiols when contacted by the tip was observed by a reduction of the oscillation amplitude from its free (noncontact) value of 10 Å peak-to-peak to ∼1−2 Å. Because in these experiments, the radius of the Pt−Rh tips was typically between 1000 Å and 1 μm (depending on preparation conditions), the thiol molecules remained trapped between tip and surface, even at pressures where the gold substrate was found to yield plastically. This occurred when the applied load became larger than ∼2 μN, corresponding to a pressure of 1−2 GPa. This plastic deformation of the Au substrate was observed as permanent indentations in subsequent AFM images acquired at zero load.[265] The images in Figure 19 show the topography of the surface of Au films on silicon substrates, before and after two indentation experiments with loads of 5 μN each. The plastic yield of the Au substrate occurs while the thiol molecules remained trapped between tip and substrate and still cushioning the oscillation to a ∼1−2 Å amplitude. The results indicates that, aside from the small oscillatory compression, the alkanethiol molecules are rigidly supporting the load. The same conclusion is inherent in the results of Thomas *et al.*[231] discussed in section IV.B.2. The right hand side of Figure 19 shows the simultaneous current images acquired by applying a small voltage (0.1 V) to the tip. The current is within the noise level of tens of picoamps in the flat terrace regions due to the insulating nature of the molecules and the low tunnel probability through them, but becomes measurable (nanoamps), at grain boundaries and near holes, indicating that in these regions the packing of the molecules is low enough to allow the tip to get closer to the surface and detect current.

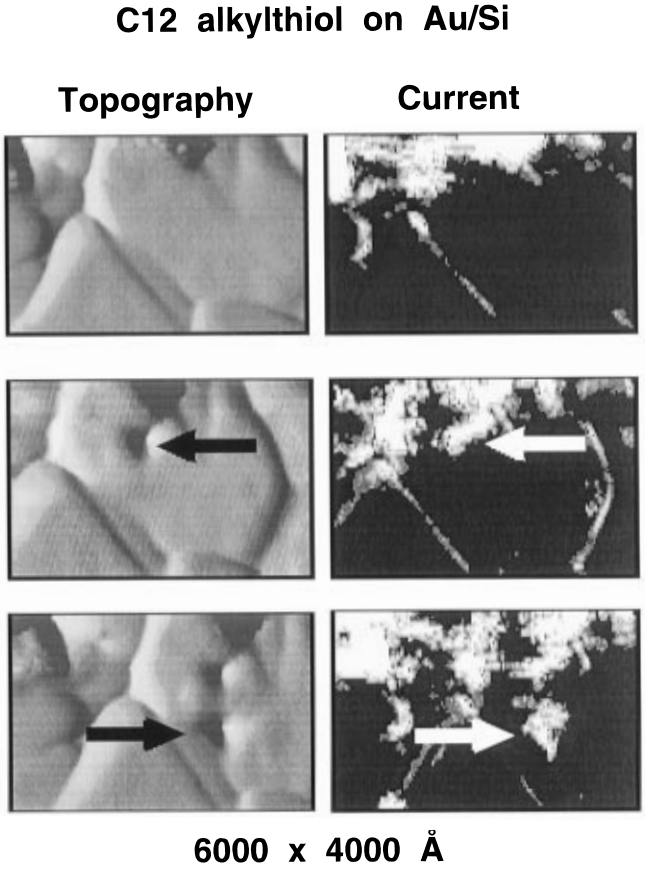

Figure 19. Indentation experiments to observe the effect of plastic deformation on gold on silicon with a $-S(CH_2)_{11}-CH_3$ monolayer. The 6000 × 4000 Å images are obtained using a noncontact topographic ac-mode and displayed light-shaded for better contrast. The surface before indentation is shown on top and after contact (below) at two loads of (5.5 and 4.5) × 10^{-6} N. The two indentation marks have depths of ∼70 Å. Current maps at 0.1V bias (right image) show current at the grain boundaries and at defective areas. Additional current is observed around the two indentation marks. (From Salmeron *et al.*[265] Copyright 1995 American Chemical Society.)

2. Sharp Tip Radii (R < 1000 Å)

A very different behavior was observed by Liu *et al.*[287] for thiols on Au, and by Xiao *et al.*[253] for siloxanes on mica, when using sharp silicon nitride

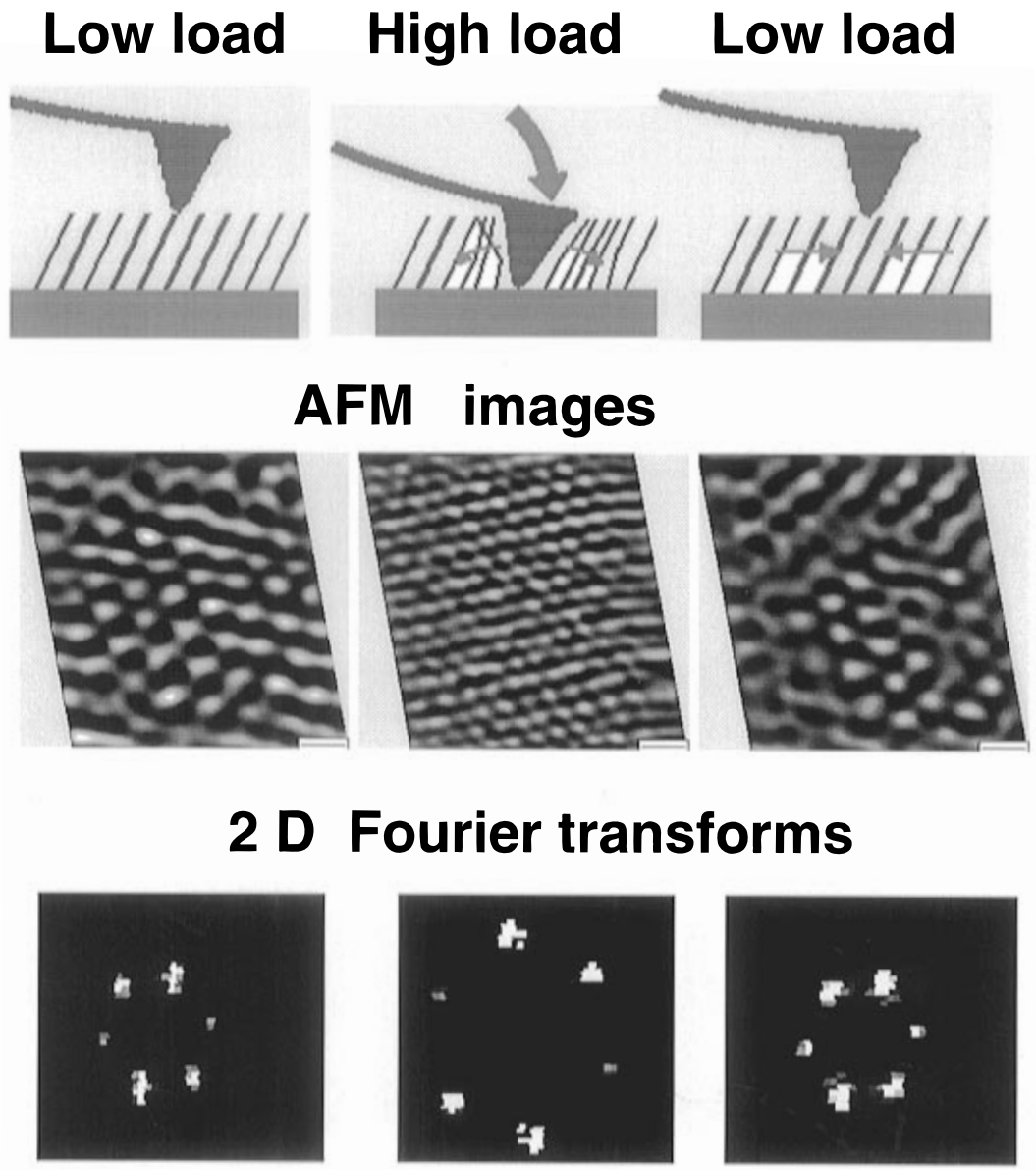

Figure 20. AFM images of a C_{18} alkanethiol monolayer at (a) low load (27 nN), (b) high load (300 nN), and (c) back to low load. Below each: two-dimensional fast-Fourier transform showing the relation between the lattices. (From Salmeron *et al.*[289] Copyright 1995 Kluwer Academic Publishers.)

tips with radii of <1000 Å. At low loads L, the response of the films was similar to the previous cases, *i.e.*, the molecules supported the load of the lever and the tip rides on top of the molecules. If the films are ordered, as in the case of the thiols on Au(111) studied here, a lattice-resolved image is obtained, as shown in Figure 20a. When the load is increased, the images retain the original ordered structure up to a critical value L_c, where the periodicity of the images changed to a new one that is characteristic of the Au(111) substrate in the case of thiols (see Figure 20b), or of the mica in the case of siloxane films. During the transition, the tip moved closer to the surface by ~25 Å, the thickness of the layer as shown by Lio *et al.*[288] Upon lowering the pressure exerted by the tip, the original ordered structure of the thiol layers on Au is recovered (Figure 20c). This was observed for all thiol molecules investigated: C_{18}, C_{12}, C_{10}, and also for fluorinated thiols.[268] Depending on the tip radius, the value of L_c could be as low as 10 nN (when the tip radius is $R \approx 100$ Å), or as high as 300 nN (for $R \approx$ 700 Å). With larger radii, no transition was observed. However, the pressure at the critical load is nearly the same for all tip radius, and of the order of 1 GPa. With silane films, no recovery upon removal of the load occurred and a permanent wear scar was left on the sample.[253]

The reversibility of the transition for the thiol films on Au is explained as a result of the lateral displacement of the molecules, which remain bonded to the Au substrate through the S end. The tip, of course, supplies the energy to overcome S diffusion barriers (on the order of 0.1 eV) and the energy to compress the thiol molecules in a region around the tip. Because of the finite lateral compressibility of the thiol alkane chains, only a relatively small number of molecules can be displaced from under the tip into the surrounding area. This explains why only sharp tips are capable of producing the transition from the thiol to the Au periodicity by displacement of the molecules. For the silane films on mica, the tip penetration and molecular displacement is only done by breaking the cross-links between molecules, a

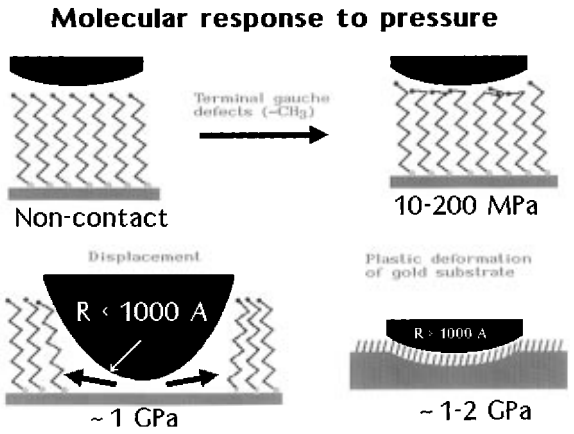

Figure 21. Schematic representation summarizing the molecular structure of model lubricant monolayers when subjected to different compressive forces. At pressures of 10−200 MPa, the molecules remain more or less normal to the surface but contain gauche defects near the free end (top right). These pressures are typically 1 order of magnitude lower than with AFM tip contact. Sharp tips might penetrate and laterally displace the molecules (bottom left) while blunt tips can trap the molecules (bottom right). Interestingly the trapped molecules can support the load beyond the plastic lmit of gold substrates.

process that is irreversible.[253] Figure 21 is a schematic representation summarizing the processes described in the previous sections.

The energetics of the displacement process can be described by a simple model that assumes elastic deformation of the tip, thiol and gold substrate on one side, and the formation of new interfaces between tip and surface as the contact area grows during compression. The first processes (elastic compression) absorb energy while the second processes (interface growth) provides energy. A more detailed description can be found in the work by Salmeron *et al.*[289]

In summary, this last section has shown that the combined application of AFM, SFA, and spectroscopies that can selectively access the buried interface can provide a detailed picture of the molecular structure in SAM and LB films that model lubricants.

VI. Conclusions

Many of the examples discussed above only demonstrate the potential of force microscopy to address problems in nanotribology, although substantial qualitative insight and some important quantitative results have emerged. Progress is expected to continue at a fast pace as technical approaches are refined, new systems are investigated and more researchers join this expanding field.

Nevertheless, the gap between macroscopic tribology and nanotribology is large and must be bridged. For example, AFM provides a unique opportunity to probe single asperity contacts, which as we previously discussed, is useful information for modeling more complicated contacts which occur in practical situations. However, the small size and high aspect ratio are not representative of all common interfacial asperities at surfaces. Also, UHV studies provide a controlled chemical environment, but it is not clear how the knowledge gained in these experiments can be extrapolated to tribological contacts operating in air, with lubricating films, contamination, and wear debris involved.

Here we summarize what we feel are important outstanding issues which need to be addressed to make progress specifically aimed at bridging this gap.

·In order to obtain *quantitative* knowledge from force microscopy, reliable force calibration must be performed to ensure accuracy. For the reasons discussed in section II.B, we are convinced that *in situ* calibration of cantilevers is necessary. Also, instrumental details discussed in section II such as normal/lateral force coupling *etc.* must be carefully considered.

·Determination of the geometry, atomic structure, and chemical composition of the tip is necessary and must be a priority in future experiments. Otherwise, half of the interface being probed remains uncertain. Experiments addressing this have been discussed above but further work is necessary. An AFM experiment with an uncharacterized tip cannot be reliably compared with theory or other experimental work. UHV experiments should attempt to take advantage of surface preparation tools such as evaporation or sputtering to prepare the tip, or analysis tools such as field ion microscopy[45] to characterize tips. Utilization of a wider variety of tip materials would also be useful. Different tip sizes should also be employed, to see how the behavior changes as the asperity size increases.

·Until the above issues are addressed, more systematic *comparative* studies using the *same* tip should be carried out, to eliminate uncertainties due to unknown tip properties.

·The contact area must be determined to understand its role in determining friction. This involves exploring (i) what determines the contact area, and (ii) what determines the shear strength. Both of these depend upon the nature of the interface, but it is not known how. Continuum models seem to be able to quantitatively predict the contact area as a function of the material elastic constants and interfacial forces. However, there is no way to predict either the value or functional form of shear strengths for a given interface. Theoretical efforts should be coupled with model experiments to address this. The new lateral stiffness technique described above provides useful insight on these questions, as it provides additional information regarding the contact area and the elastic constants of the materials. Measurements of contact conductance provide another method to determine the contact area, in the case of conducting tip and samples. These techniques should therefore be used in tandem with friction measurements whenever possible.

·Atomic scale stick−slip behavior must be examined more closely as its occurrence is quite general. How does atomic-scale stick−slip behavior depend upon the tip structure? Does atomic-scale stick−slip behavior imply that the (disordered?) tip atoms are being pulled into registry with the ordered sample atoms? What determines the atomic-scale stick−slip periodicity? Attempts to address these questions are needed.

·Wear processes must be considered in more detail. Is low-load friction truly wearless, or is the creation of point defects and atom transfer contributing to the energy dissipation? Can we use force microscopy and related techniques to learn about these processes? The metal nanocontact experiments[236,237,239] discussed above suggests that indeed this is the case.

·The selective wear of lubricants is a key issue since this determines the effectiveness of lubricant films to protect materials in contact. Force microscopy experiments should continue to address this question in detail.

·The behavior of confined liquids at the nanometer scale has been shown to differ substantially from bulk behavior, and this has implications for understanding lubrication. Further AFM studies in liquid environments along the lines of those discussed above would be useful.

·The processes by which energy is dissipated needs to be examined. The QCM experiments allow comparisons to models of friction entailing phononic and electronic energy dissipation mechanisms. Researchers should consider designing experiments where these kinds of contributions can be examined with AFM as well. It would be interesting to see if frictional properties changed in a system where energy-dissipating modes are altered, perhaps by changing the temperature to freeze out phonon modes, for example.

·Closer ties between experimental and theoretical work must be forged. There are few cases where the experimental conditions as well as the tip and sample materials used in experiments match with those used in theoretical models. Theorists and experimentalists alike should strive to make their respective work match more closely in this fashion.

Certainly these are not simple problems to address, but doing so is crucial if we are to progress toward better, consistent atomic-scale theories of tribology. Despite the many questions which still remain, one thing is certain: advances in force microscopy have established that picturing the complex processes taking place at a buried interface is no longer confined to the imagination.

VII. Acknowledgments

Many thoughts, insights, suggestions, and conclusions in this review were spawned from research by and discussions with the following people: Dr. D. F. Ogletree, Dr. X.-d. Xiao, Dr. J. Hu, Dr. Q. Du, Dr. C. Morant, Dr. F. Wolf, Dr. Q. Dai, Dr. R. Völlmer, Dr. P. Frantz, Dr. A. Artsyukhovich, Professor N. Agraït, Dr. D. Charych, and Professor Y. R. Shen. We thank Professor A. Searcy, Dr. M. Enachescu, and Mr. D. Schleef for corrections and improvements arising from their reading of the manuscript. We thank Ms. M. Lum for assistance with preparation of the manuscript. We thank the authors who provided us with copies of figures from their papers for this review. R.W.C. acknowledges the support of the Natural Sciences and Engineering Research Council of Canada. This work was supported by the Director, Office of Energy Research, Basic Energy Sciences, Materials Division of the US Department of Energy under contract number DE-AC03-76SF00098.

VIII. References

(1) Binnig, G.; Quate, C. F.; Gerber, C. *Phys. Rev. Lett.* **1986**, *56*, 930.
(2) Mate, C. M.; McClelland, G. M.; Erlandsson, R.; Chiang, S. *Phys. Rev. Lett.* **1987**, *59*, 1942.
(3) Bhushan, B.; Israelachvili, J. N.; Landman, U. *Nature* **1995**, *374*, 607.
(4) Krim, J. *Comments Condens. Matter. Phys.* **1995**, *17*, 263.
(5) Krim, J. *Sci. Am.* **1996**, *275*, 74.
(6) *Fundamentals of Friction: Macroscopic and Microscopic Processes*; Singer, I. L., Pollock, H. M., Eds.; Kluwer: Dordrecht, 1992.
(7) *Physics of Sliding Friction*; Persson, B. N. J., Tosatti, E., Eds.; Kluwer: Dordrecht, 1996.
(8) *Langmuir* **1996**, *12*, 4481.
(9) Dowson, D. *History of Tribology*; Longman: London, 1979.
(10) Jost, H. P. *Wear* **1990**, *136*, 1.
(11) Hutchings, I. M. *Tribology*; CRC press: Boca Raton, 1992.
(12) Howe, R. T.; Muller, R. S.; Gabriel, K. J.; Trimmer, W. S. N. *IEEE Spectrum* **1990**, *27*, 29.
(13) Grochowski, E.; Hoyt, R. F. *IEEE Trans. Magr.* **1995**, *32*, 1850.
(14) Maboudian, R.; Howe, R. T. *J. Vac. Sci. Technol. B* **1997**, *15*, 1.
(15) Bowden, F. P.; Tabor, D. *Friction and Lubrication of Solids: Part I*; Oxford University Press, 1950.
(16) Bowden, F. P.; Tabor, D. *Friction and Lubrication of Solids: Part II*; Oxford University Press, 1964.
(17) Bhushan, B. *Handbook of Micro/Nanotribology*; Chemical Rubber: Boca Rotan, 1995.
(18) Greenwood, J. A.; Williamson, J. B. P. *Proc. R. Soc. London A* **1966**, *295*, 300.
(19) Greenwood, J. A. *Fundamentals of Friction*; Singer, I. L., Pollock, H. M., Eds.; Kluwer: Dordrecht, 1992; p 37.
(20) Kim, D. E.; Suh, N. P. *Wear* **1991**, *149*, 199.
(21) Daly, C.; Krim, J. *Surf. Sci.* **1996**, *368*, 49.
(22) Persson, B. N. J. *Comments Condens. Matter. Phys.* **1995**, *17*, 281.
(23) Sokoloff, J. B. *Phys. Rev. B* **1995**, *52*, 5318.
(24) Persson, B. N. J.; Volokitin, A. I. *J. Chem. Phys.* **1995**, *103*, 8679.
(25) Persson, B. N. J.; Nitzan, A. *Surf. Sci.* **1996**, *367*, 261.
(26) Sokoloff, J. B. *Wear* **1993**, *167*, 59.
(27) Krim, J.; Solina, D. H.; Chiarello, R. *Phys. Rev. Lett.* **1991**, *66*, 181.
(28) Watts, E. T.; Krim, J.; Widom, A. *Phys. Rev. B* **1990**, *41*, 3466.
(29) Daly, C.; Krim, J. *Phys. Rev. Lett.* **1996**, *76*, 803.
(30) Tabor, D.; Winterton, R. H. S. *Proc. R. Soc. London A* **1969**, *312*, 435.
(31) Israelachvili, J. N.; Tabor, D. *Proc. R. Soc. London A* **1972**, *331*, 19.
(32) Israelachvili, J. N.; McGuiggan, P. M.; Homola, A. M. *Science* **1988**, *240*, 189.
(33) Peachey, J.; Van Alsten, J.; Granick, S. *Rev. Sci. Instrum.* **1991**, *62*, 463.
(34) Harrison, J. A.; Brenner, D. W. *Handbook of Micro/Nanotribology*; Bhushan, B., Ed.; CRC Press: Boca Raton, 1995; p 397.
(35) Marti, O.; Drake, B.; Hansma, P. K. *Appl. Phys. Lett.* **1987**, *51*, 484.
(36) Meyer, G.; Amer, N. M. *Appl. Phys. Lett.* **1990**, *56*, 2100.
(37) Germann, G. J.; Cohen, S. R.; Neubauer, G.; McClelland, G. M.; Seki, H.; Coulman, D. *J. Appl. Phys.* **1993**, *73*, 163.
(38) Howald, L.; Meyer, E.; Lüthi, R.; Haefke, H.; Overney, R.; Rudin, H.; Güntherodt, H.-J. *Appl. Phys. Lett.* **1993**, *63*, 117.
(39) Kageshima, M.; Yamada, H.; Nakayama, K.; Sakama, H.; Kawau, A.; Fujii, T.; Suzuki, M. *J. Vac. Sci. Technol. B* **1993**, *11*, 1987.
(40) Park Scientific Instruments Inc., Sunnyvale, CA.
(41) Digital Instruments Inc., Santa Barbara, CA.
(42) Nanosensors GmbH, Aidlingen, Germany.
(43) Olympus Optical Company, Japan.
(44) Lu, C.-J.; Jiang, Z.; Bogy, D. B.; Miyamoto, T. *Trans. ASME J. Tribol.* **1995**, *117*, 244.
(45) Enachescu, M.; Smallwood, S. A.; Lad, R. J.; Unertl, W. N. Manuscript in preparation.
(46) Alexander, S.; Hellemans, L.; Marti, O.; Schneir, J.; Elings, V.; Hansma, P. K.; Longmire, M.; Gurley, J. *J. Appl. Phys.* **1989**, *65*, 164.
(47) Marti, O.; Colchero, J.; Mlynek, J. *Nanotechnology* **1991**, *1*, 141.
(48) Kolbe, W. F.; Ogletree, D. F.; Salmeron, M. B. *Ultramicroscopy* **1992**, *42*−44, pt.B, 1113.
(49) Dai, Q.; Vollmer, R.; Carpick, R. W.; Ogletree, D. F.; Salmeron, M. *Rev. Sci. Instrum.* **1995**, *66*, 5266.
(50) Radmacher, M.; Cleveland, J. P.; Hansma, P. K. *Scanning* **1995**, *17*, 117.
(51) Morita, S.; Fujisawa, S.; Sugawara, Y. *Surf. Sci. Rep.* **1996**, *23*, 3.
(52) Jaschke, M.; Butt, H. J. *Rev. Sci. Instrum.* **1995**, *66*, 1258.
(53) Martin, Y.; Williams, C. C.; Wickramasinghe, H. K. *J. Appl. Phys.* **1987**, *61*, 4723.
(54) Rugar, D.; Mamin, H. J.; Güthner, P. *Appl. Phys. Lett.* **1989**, *55*, 2588.

(55) Schonenberger, C.; Alvarado, S. F. *Rev. Sci. Instrum.* **1989**, *60*, 3131.
(56) Erlandsson, R.; McClelland, G. M.; Mate, C. M.; Chiang, S. *J. Vac. Sci. Technol. A* **1988**, *6*, 266.
(57) Goddenhenrich, T.; Muller, S.; Heiden, C. *Rev. Sci. Instrum.* **1994**, *65*, 2870.
(58) Linnemann, R.; Gotszalk, T.; Rangelow, I. W.; Dumania, P.; Oesterschulze, E. *J. Vac. Sci. Technol. B* **1996**, *14*, 856.
(59) Bartzke, K.; Antrack, T.; Schmidt, K.-H.; Dammann, E.; Schatterny, C. *Int. J. Optoelectron.* **1993**, *8*, 669.
(60) Murdfield, T.; Fischer, U. C.; Fuchs, H.; Volk, R.; Michels, A.; Meinen, F.; Beckman, E. *J. Vac. Sci. Technol. B* **1996**, *14*, 877.
(61) Güthner, P.; Fischer, U. C.; Dransfeld, K. *Appl. Phys. B* **1989**, *48*, 89.
(62) Ogletree, D. F.; Carpick, R. W.; Salmeron, M. *Rev. Sci. Instrum.* **1996**, *67*, 3298.
(63) Bhushan, B.; Ruan, J. A. *Trans. ASME J. Tribol.* **1994**, *116*, 389.
(64) Ascoli, C.; Dinelli, F.; Frediani, C.; Petracchi, D.; Salerno, M.; Labardi, M.; Allegrini, M.; Fuso, F. *J. Vac. Sci. Technol. B* **1993**, *12*, 1642.
(65) Timoshenko, S. P.; Goodier, J. N. *Theory of Elasticity*; McGraw Hill: New York, 1987.
(66) Albrecht, T. R.; Akamine, S.; Carver, T. E.; Quate, C. F. *J. Vac. Sci. Technol. A* **1990**, *8*, 3386.
(67) Butt, H.-J.; Siedle, P.; Seifert, K.; Fendler, K.; Seeger, T.; Bamberg, E.; Weisenhorn, A. L.; Goldie, K.; Engel, A. *J. Microsc.* **1993**, *169*, 75.
(68) Neumeister, J. M.; Ducker, W. A. *Rev. Sci. Instrum.* **1994**, *65*, 2527.
(69) Sader, J. E. *Rev. Sci. Instrum.* **1995**, *66*, 4583.
(70) Lüthi, R.; Meyer, E.; Haefke, H.; Howald, L.; Gutmannsbauer, W.; Guggisberg, M.; Bammerlin, M.; Güntherodt, H.-J. *Surf. Sci.* **1995**, *338*, 247.
(71) Sader, J. E.; Larson, I.; Mulvaney, P.; White, L. R. *Rev. Sci. Instrum.* **1995**, *66*, 3789.
(72) Schwarz, U. D.; Koster, P.; Wiesendanger, R. *Rev. Sci. Instrum.* **1996**, *67*, 2560.
(73) Cleveland, J. P.; Manne, S.; Bocek, D.; Hansma, P. K. *Rev. Sci. Instrum.* **1993**, *64*, 403.
(74) Senden, T. J.; Ducker, W. A. *Langmuir* **1994**, *10*, 1003.
(75) Torii, A.; Sasaki, M.; Hane, K.; Okuma, S. *Meas. Sci. Technol.* **1996**, *7*, 179.
(76) Ruan, J. A.; Bhushan, B. *Trans. ASME J. Tribol.* **1994**, *116*, 378.
(77) Li, Y. Q.; Tao, N. J.; Pan, J.; Garcia, A. A.; Lindsay, S. M. *Langmuir* **1993**, *9*, 637.
(78) Butt, H. J.; Jaschke, M. *Nanotechnology* **1995**, *6*, 1.
(79) Hutter, J. L.; Bechhoefer, J. *Rev. Sci. Instrum.* **1993**, *64*, 1868.
(80) Staub, R.; Alliata, D.; Nicolini, C. *Rev. Sci. Instrum.* **1995**, *66*, 2513.
(81) Hues, S. M.; Draper, C. F.; Lee, K. P.; Colton, R. J. *Rev. Sci. Instrum.* **1994**, *65*, 1561.
(82) Fu, J. *Rev. Sci. Instrum.* **1995**, *66*, 3785.
(83) Nagahara, L. A.; Hashimoto, K.; Fujishima, A.; Snowden-Ifft, D.; Price, P. B. *J. Vac. Sci. Technol. B* **1993**, *12*, 1694.
(84) Brodowsky, H. M.; Boehnke, U.-C.; Kremer, F. *Rev. Sci. Instrum.* **1996**, *67*, 4198.
(85) Carpick, R. W.; Agraït, N.; Ogletree, D. F.; Salmeron, M. *J. Vac. Sci. Technol. B* **1996**, *14*, 1289.
(86) Jarausch, K. F.; Stark, T. J.; Russell, P. E. *J. Vac. Sci. Technol. B* **1996**, *14*, 3425.
(87) Atamny, F.; Baiker, A. *Surf. Sci.* **1995**, *323*, L314.
(88) Sheiko, S. S.; Moller, M.; Reuvekamp, E. M. C. M.; Zandbergen, H. W. *Ultramicroscopy* **1994**, *53*, 371.
(89) Odin, C.; Aime, J. P.; El Kaakour, Z.; Bouhacina, T. *Surf. Sci.* **1994**, *317*, 321.
(90) Westra, K. L.; Thomson, D. J. *J. Vac. Sci. Technol. B* **1994**, *12*, 3176.
(91) Markiewicz, P.; Goh, M. C. *Rev. Sci. Instrum.* **1995**, *66*, 3186.
(92) Dixson, R.; Schneir, J.; McWaid, T.; Sullivan, N.; Tsai, V. W.; Zaidi, S. H.; Brueck, S. R. J. *Proc. SPIE - Int. Soc. Opt. Eng.* **1996**, *2725*, 589.
(93) Siedle, P.; Butt, H.-J.; Bamberg, E.; Wang, D. N.; Kuhlbrandt, W.; Zach, J.; Haider, M. *X-ray Optics and Microanalysis, 1992.*; Kenway, P. B., Duke, P. J., Lorimer, G. W., *et al.*, Eds.; Iop: Manchester, UK, 1992; p 361.
(94) Xu, S.; Arnsdorf, M. F. *J. Microsc.* **1994**, *3*, 199.
(95) Schwarz, U. D.; Zwörner, O.; Köster, P.; Wiesendanger, R. *Micro/Nanotribology and Its Applications*; Bhushan, B., Ed.; Kluwer Academic Publishers: Dordrecht, 1997.
(96) O'Shea, S. J.; Atta, R. N.; Welland, M. E. *Rev. Sci. Instrum.* **1995**, *66*, 2508.
(97) Niedermann, P.; Hanni, W.; Blanc, N.; Christoph, R.; Burger, J. *J. Vac. Sci. Technol. A* **1995**, *14*, 1233.
(98) Giessibl, F. J. *Science* **1995**, *267*, 68.
(99) Overney, R. M.; Meyer, E.; Frommer, J.; Brodbeck, D.; Lüthi, R.; Howald, L.; Güntherodt, H.-J.; Fujihara, M.; Takano, H.; Gotoh, Y. *Nature* **1992**, *359*, 133.
(100) Frisbie, C. D.; Rozsnyai, L. F.; Noy, A.; Wrighton, M. S.; Lieber, C. M. *Science* **1994**, *265*, 2071.
(101) Carpick, R. W.; Dai, Q.; Ogletree, D. F.; Salmeron, M. Manuscript in preparation.
(102) Hu, J.; Xiao, X.-D.; Ogletree, D. F.; Salmeron, M. *Surf. Sci.* **1995**, *327*, 358.
(103) Maivald, P.; Butt, H. J.; Gould, S. A. C.; Prater, C. B.; Drake, B.; Gurley, J. A.; Elings, V. B.; Hansma, P. K. *Nanotechnology* **1991**, *2*, 103.
(104) Radmacher, M.; Tillmann, R. W.; Fritz, M.; Gaub, H. E. *Science* **1992**, *257*, 1900.
(105) Overney, R. M.; Takano, H.; Fujihira, M. *Europhys. Lett.* **1994**, *26*, 443.
(106) Heuberger, M.; Dietler, G.; Schlapbach, L. *Nanotechnology* **1995**, *6*, 12.
(107) Hoper, R.; Gesang, T.; Possart, W.; Hennemann, O.-D.; Boseck, S. *Ultramicroscopy* **1995**, *60*, 17.
(108) Kajiyama, T.; Ohki, I.; Tanaka, K.; Ge, S.-R.; Takahara, A. *Proc. Jpn. Acad. B* **1995**, *71*, 75.
(109) Yamanaka, K.; Ogiso, H.; Kolosov, O. *Appl. Phys. Lett.* **1994**, *64*, 178.
(110) Kolosov, O.; Yamanaka, K. *Jpn. J. Appl. Phys. 2, Lett.* **1993**, *32*, L1095.
(111) Jarvis, S. P.; Oral, A.; Weihs, T. P.; Pethica, J. B. *Rev. Sci. Instrum.* **1993**, *64*, 3515.
(112) Jarvis, S. P.; Yamada, H.; Yamamoto, S.-I.; Tokumoto, H. *Rev. Sci. Instrum.* **1996**, *67*, 2281.
(113) Joyce, S. A.; Houston, J. E. *Rev. Sci. Instrum.* **1991**, *62*, 710.
(114) Joyce, S. A.; Houston, J. E.; Michalske, T. A. *Appl. Phys. Lett.* **1992**, *60*, 1175.
(115) Burnham, N. A.; Colton, R. J. *J. Vac. Sci. Technol. A* **1989**, *7*, 2906.
(116) Burnham, N. A.; Colton, R. J.; Pollock, H. M. *Nanotechnology* **1993**, *4*, 64.
(117) Pethica, J. B.; Sutton, A. P. *J. Vac. Sci. Technol. A* **1988**, *6*, 2494.
(118) Bhushan, B.; Koinkar, V. N. *Appl. Phys. Lett.* **1994**, *64*, 1653.
(119) Lu, C. J.; Bogy, D.; Kaneko, R. *Trans. ASME J. Tribol.* **1994**, *116*, 175.
(120) Jarvis, S. P.; Pethica, J. B. *Thin Solid Films* **1996**, *273*, 284.
(121) O'Shea, S. J. W., M. E.; Pethica, J. B. *Chem. Phys. Lett.* **1994**, *223*, 336.
(122) Landman, U.; Luedtke, W. D.; Gao, J. P. *Langmuir* **1996**, *12*, 4514.
(123) Israelachvili, J. N. *Intermolecular and surface forces*, 2nd ed.; Academic Press London: London, 1992.
(124) Dowson, D.; Higginson, G. R. *Elasto-hydrodynamic lubrication*; Pergamon Press: Oxford, 1977.
(125) Carpick, R. W.; Ogletree, D. F.; Salmeron, M. *Appl. Phys. Lett.* **1997**, *70*.
(126) Yamanaka, K.; Tomita, E. *Jpn. J. Appl. Phys. 1, Regul. Pap.* **1995**, *34*, 2879.
(127) Lantz, M. A.; O'Shea, S. J.; Hoole, A. C. F.; Welland, M. E. *Appl. Phys. Lett.* **1997**, *70*, 970.
(128) Johnson, K. L. *Contact Mechanics*; University Press: Cambridge, 1987.
(129) Fujisawa, S.; Kishi, E.; Sugawara, Y.; Morita, S. *Appl. Phys. Lett.* **1995**, *66*, 526.
(130) Israelachvili, J. N. *J. Colloid Interface Sci.* **1973**, *44*, 259.
(131) Frantz, P.; Agraït, N.; Salmeron, M. *Langmuir* **1996**, *12*, 3289.
(132) Chan, D. Y. C.; Horn, R. G. *J. Chem. Phys.* **1985**, *83*, 5311.
(133) Klein, J.; Kumacheva, E. *Science* **1995**, *269*, 816.
(134) Lu, C.; Czanderna, A. W. *Applications of Piezoelectric Quartz Crystal Microbalances*; Elsevier: Amsterdam, 1984.
(135) Krim, J.; Widom, A. *Phys. Rev. B* **1988**, *38*, 12184.
(136) Krim, J.; Chiarello, R. *J. Vac. Sci. Technol. A* **1991**, *9*, 2566.
(137) Cieplak, M.; Smith, E. D.; Robbins, M. O. *Science* **1994**, *265*, 1209.
(138) Takano, H.; Fujihira, M. *J. Vac. Sci. Technol. B* **1996**, *14*, 1272.
(139) Howald, L.; Lüthi, R.; Meyer, E.; Güntherodt, H.-J. *Phys. Rev. B* **1995**, *51*, 5484.
(140) Berman, A. D.; Ducker, W. A.; Israelachvili, J. N. *Langmuir* **1996**, *12*, 4559.
(141) Tomanek, D.; Zhong, W.; Thomas, H. *Europhys. Lett.* **1991**, *15*, 887.
(142) Sokoloff, J. B. *Thin Solid Films* **1991**, *206*, 208.
(143) McClelland, G. M.; Glosli, J. N. *Fundamentals of Friction*; Singer, I. L., Pollock, H. M., Eds.; Kluwer: Dordrecht, 1992; p 405.
(144) Kerssemakers, J.; De Hosson, J. T. M. *Appl. Phys. Lett.* **1995**, *67*, 347.
(145) Gyalog, T.; Bammerlin, M.; Lüthi, R.; Meyer, E.; Thomas, H. *Europhys. Lett.* **1995**, *31*, 269.
(146) Sasaki, N.; Kobayashi, K.; Tsukada, M. *Jpn. J. Appl. Phys. 1* **1996**, *35*, 3700.
(147) Hölscher, H.; Schwarz, U. D.; Wiesendanger, R. *Europhys. Lett.* **1996**, *36*, 19.
(148) Gyalog, T.; Thomas, H. *Physics of sliding friction*; Persson, B. N. J., Tosatti, E., Eds.; Kluwer Academic Publishers: Dordrecht, 1996; p 403.
(149) Kerssemakers, J.; De Hosson, J. T. M. *J. Appl. Phys.* **1996**, *80*, 623.

(150) Weiss, M.; Elmer, F.-J. *Phys. Rev. B* **1996**, *53*, 7539.
(151) Sasaki, N.; Kobayashi, K.; Tsukada, M. *Surf. Sci.* **1996**, *357*−358, 92.
(152) Colchero, J.; Baro, A. M.; Marti, O. *Tribol. Lett.* **1996**, *2*, 327.
(153) Gyalog, T.; Thomas, H. *Europhys. Lett.* **1997**, *37*, 195.
(154) Harrison, J. A.; White, C. T.; Colton, R. J.; Brenner, D. W. *Phys. Rev. B* **1992**, *46*, 9700.
(155) Perry, M. D.; Harrison, J. A. *J. Phys. Chem.* **1995**, *99*, 9960.
(156) Sørensen, M. R.; Jacobsen, K. W.; Stoltze, P. *Phys. Rev. B* **1996**, *53*, 2101.
(157) Shluger, A. L.; Williams, R. T.; Rohl, A. L. *Surf. Sci.* **1995**, *343*, 273.
(158) McClelland, G. M. *Adhesion and Friction*; Springer Series in Surface Science, Springer: New York, 1989; Vol. 17; p 1.
(159) Landman, U.; Luedtke, W. D.; Nitzan, A. *Surf. Sci. Lett.* **1989**, *210*, L177.
(160) Landman, U.; Luedtke, W. D.; Ribarsky, M. W. *J. Vac. Sci. Technol. A* **1989**, *7*, 2829.
(161) Tomlinson, G. A. *Philos. Mag.* **1929**, *7*, 905.
(162) Sokoloff, J. B. *Phys. Rev. Lett.* **1993**, *71*, 3450.
(163) Sokoloff, J. B. *Phys. Rev. B* **1995**, *52*, 7205.
(164) Lüthi, R.; Meyer, E.; Bammerlin, M.; Howald, L.; Haefke, H.; Lehmann, T.; Loppacher, C.; Güntherodt, H.-J.; Gyalog, T.; Thomas, H. *J. Vac. Sci. Technol. B* **1996**, *14*, 1280.
(165) Landman, U.; Luedtke, W. D. *Scanning tunneling microscopy III: theory of STM and related scanning probe methods*; Wiesendanger, R., Guntherodt, H.-J., Eds.; Springer-Verlag: Berlin, 1993; p 207.
(166) Yoshizawa, H.; Chen, Y.-L.; Israelachvili, J. *Wear* **1993**, *168*, 161.
(167) Reiter, G.; Demirel, A. L.; Peanasky, J.; Cai, L. L.; Granick, S. *J. Chem. Phys.* **1994**, *101*, 2606.
(168) Reiter, G.; Demirel, A. L.; Granick, S. *Science* **1994**, *263*, 1741.
(169) Howald, L.; Lüthi, R.; Meyer, E.; Gerth, G.; Haefke, H.; Overney, R.; Güntherodt, H.-J. *J. Vac. Sci. Technol. B* **1994**, *12*, 2227.
(170) Giessibl, F. J.; Binnig, G. *Ultramicroscopy* **1991**, *42*−44, 281.
(171) Putman, C. A. J.; Igarashi, M.; Kaneko, R. *Appl. Phys. Lett.* **1995**, *66*, 3221.
(172) Carpick, R. W.; Agraït, N.; Ogletree, D. F.; Salmeron, M. *Langmuir* **1996**, *12*, 3334.
(173) Meyer, E.; Lüthi, R.; Howald, L.; Bammerlin, M.; Guggisberg, M.; Güntherodt, H.-J. *J. Vac. Sci. Technol. B* **1996**, *14*, 1285.
(174) Schwarz, U. D.; Allers, W.; Gensterblum, G.; Wiesendanger, R. *Phys. Rev. B* **1995**, *52*, 14976.
(175) Homola, A. M.; Israelachvili, J. N.; McGuiggan, P. M.; Gee, M. L. *Wear* **1990**, *136*, 65.
(176) Homola, A. M.; Israelachvili, J. N.; Gee, M. L.; McGuiggan, P. M. *J. Tribology* **1989**, *111*, 675.
(177) Hertz, H. *J. Reine Angew. Math.* **1881**, *92*, 156.
(178) Israelachvili, J. N. *Fundamentals of Friction*; Singer, I. L., Pollock, H. M., Eds.; Kluwer: Dordrecht, 1992; p 351.
(179) Briscoe, B. J.; Evans, D. C. B. *Proc. R. Soc. London A* **1982**, *380*, 389.
(180) Johnson, K. L.; Kendall, K.; Roberts, A. D. *Proc. R. Soc. London A* **1971**, *324*, 301.
(181) Derjaguin, B. V.; Muller, V. M.; Toporov, Y. P. *J. Colloid Interface Sci.* **1975**, *53*, 314.
(182) Müller, V. M.; Yushenko, V. S.; Derjaguin, B. V. *J. Colloid Interface Sci.* **1980**, *77*, 91.
(183) Maugis, D. *J. Colloid Interface Sci.* **1992**, *150*, 243.
(184) Johnson, K. L.; Greenwood, J. A. *J. Colloid Interface Sci.*, submitted.
(185) Fogden, A.; White, L. R. *J. Colloid Interface Sci.* **1990**, *138*, 414.
(186) Johnson, K. L. *Proc. R. Soc. London A* **1997**, *A453*, 163.
(187) Sheiko, S. S.; Möller, M.; Reuvekamp, E. M. C. M.; Zandbergen, H. W. *Phys. Rev. B* **1993**, *48*, 5675.
(188) Lüthi, R.; Meyer, E.; Haefke, H.; Howald, L.; Gutmannsbauer, W.; Güntherodt, H.-J. *Science* **1994**, *266*, 1979.
(189) Sheehan, P. E.; Lieber, C. M. *Science* **1996**, *272*, 1158.
(190) Meyer, E.; Overney, R.; Brodbeck, D.; Howald, L.; Lüthi, R.; Frommer, J.; Güntherodt, H.-J. *Phys. Rev. Lett.* **1992**, *69*, 1777.
(191) Christenson, H. K. *J. Phys. Chem.* **1993**, *97*, 12034.
(192) Agrawal, D. C.; Raj, R. *Acta Metall.* **1989**, *37*, 1265.
(193) Timsit, R. S. *Fundamentals of Friction*; Singer, I. L., Pollock, H. M., Eds.; Kluwer: Dordrecht, 1992; p 287.
(194) Singer, I. L.; Bolster, R. N.; Wegand, J.; Fayeulle, S.; Stupp, B. C. *Appl. Phys. Lett.* **1990**, *57*, 995.
(195) Fuller, K. N. G.; Tabor, D. *Proc. R. Soc. London A* **1975**, *345*, 327.
(196) Bluhm, H.; Schwarz, U. D.; Meyer, K. P.; Wiesendanger, R. *Appl. Phys. A* **1995**, *61*, 525.
(197) Schwarz, U. D.; Bluhm, H.; Hölscher, H.; Allers, W.; Wiesendanger, R. *Physics of sliding friction*; Persson, B. N. J., Tosatti, E., Eds.; Kluwer Academic Publishers: Dordrecht, 1996; p 369.
(198) Overney, R. M.; Takano, H.; Fujihira, M.; Paulus, W.; Ringsdorf, H. *Phys. Rev. Lett.* **1994**, *72*, 3546.
(199) Gruner, G.; Zettl, A. *Phys. Rep.* **1985**, *119*, 117.
(200) Shinjo, K.; Hirano, M. *Surf. Sci.* **1993**, *283*, 473.
(201) Hirano, M.; Shinjo, K.; Kaneko, R.; Murata, Y. *Phys. Rev. Lett.* **1991**, *67*, 2642.
(202) Sutton, A. P.; Balluffi, R. W. *Interfaces in Crystalline Materials*; Oxford University Press: Oxford, 1995.
(203) Marti, A.; Hahner, G.; Spencer, N. D. *Langmuir* **1995**, *11*, 4632.
(204) Binggeli, M.; Christoph, R.; Hintermann, H.-E. *Tribol. Lett.* **1995**, *1*, 13.
(205) Binggeli, M.; Mate, C. M. *Appl. Phys. Lett.* **1994**, *65*, 415.
(206) Schumacher, A.; Kruse, N.; Prins, R.; Meyer, E.; Lüthi, R.; Howald, L.; Güntherodt, H.-J.; Scandella, L. *J. Vac. Sci. Technol. B* **1996**, *14*, 1264.
(207) Rabinowicz, E. *Friction and Wear of Materials*, 2nd ed.; Wiley: New York, 1995.
(208) Khurshudov, A.; Kato, K. *J. Vac. Sci. Technol. B* **1995**, *13*, 1938.
(209) Kaneko, R.; Miyamoto, T.; Andoh, Y.; Hamada, E. *Thin Solid Films* **1996**, *273*, 105.
(210) Wei, B.; Komvopoulos, K. *Trans. ASME J. Tribology* **1995**, *117*, 594.
(211) Bhushan, B.; Koinkar, V. N. *J. Appl. Phys.* **1994**, *75*, 5741.
(212) Bhushan, B.; Kulkarni, A. V. *Thin Solid Films* **1996**, *278*, 49.
(213) Bhushan, B. *Proceedings of IEEE, 9th Annual International Workshop on Micro Electro Mechanical Systems, An Investigation of Micro Structures, Sensors, Actuators, Machines and Systems*; IEEE: New York, 1996.
(214) Miyamoto, T.; Serikawa, T.; Hirono, S.; Jiang, Z.; Bogy, D. B.; Kaneko, R. *IEEE Trans. Magr.* **1995**, *31*, 3018.
(215) Jiang, Z.; Lu, C.-J.; Bogy, D. B.; Miyamoto, T. *Trans. ASME J. Tribol.* **1995**, *117*, 328.
(216) Lu, C.-J.; Jiang, Z.; Bogy, D. B.; Miyamoto, T. *Trans. ASME J. Tribol.* **1995**, *117*, 334.
(217) Zhaoguo, J.; Lu, C. J.; Bogy, D. B.; Bhatia, C. S.; Miyamoto, T. *Thin Solid Films* **1995**, *258*, 75.
(218) Miyake, S. *Appl. Phys. Lett.* **1994**, *65*, 980.
(219) Miyake, S. *Appl. Phys. Lett.* **1995**, *67*, 2925.
(220) Nakahara, S.; Langford, S. C.; Dickinson, J. T. *Tribol. Lett.* **1995**, *1*, 277.
(221) Khurshudov, A.; Kato, K. *Ultramicroscopy* **1995**, *60*, 11.
(222) Khurshudov, A. G.; Kato, K.; Koide, H. *Tribol. Lett.* **1996**, *2*, 345.
(223) Shluger, A. L.; Rohl, A. L.; Williams, R. T.; Wilson, R. M. *Phys. Rev. B* **1995**, *52*, 11398.
(224) Harrison, J. A.; White, C. T.; Colton, R. J.; Brenner, D. W. *Surf. Sci.* **1992**, *271*, 57.
(225) Landman, U.; Luedtke, W. D.; Ringer, E. M. *Wear* **1992**, *153*, 3.
(226) Thundat, T.; Sales, B. C.; Chakoumakos, B. C.; Boatner, L. A.; Allison, D. P.; Warmack, R. J. *Surf. Sci.* **1993**, *293*, L863.
(227) Kim, Y.; Huang, J. L.; Lieber, C. M. *Appl. Phys. Lett.* **1991**, *59*, 3404.
(228) Hirvonen, J. P.; Koskinen, J.; Jervis, J. R.; Nastasi, M. *Surf. Coat. Technol.* **1996**, *80*, 139.
(229) Singer, I. L.; Fayeulle, S.; Ehni, P. D. *Wear* **1996**, *195*, 7.
(230) Winter, W. O. *Wear* **1967**, *10*, 422.
(231) Thomas, R. C.; Houston, J. E.; Michalske, T. A.; Crooks, R. M. *Science* **1993**, *259*, 1883.
(232) Kelly, A. *Strong Solids*, 2nd ed.; Oxford University Press: London, 1973.
(233) Macmillan, N. H. *Ideal Strength of Solids*; Latanision, R. M., Pickens, J. R., Eds.; Plenum: New York, 1981.
(234) Salmeron, M.; Folch, A.; Neubauer, G.; Tomitori, M.; Ogletree, D. F.; Kolbe, W. *Langmuir* **1992**, *8*, 2832.
(235) Sutton, A. P.; Pethica, J. B. *J. Phys., Condens. Matter.* **1990**, *2*, 5317.
(236) Rubio, G.; Agraït, N.; Vieira, S. *Phys. Rev. Lett.* **1996**, *76*, 2602.
(237) Agraït, N.; Rubio, G.; Vieira, S. *Phys. Rev. Lett.* **1994**, *74*, 3995.
(238) Dürig, U. *Physics of Sliding Friction*; Persson, B. N. J., Tosatti, E., Eds.; Kluwer: Dordrecht, 1996; p 299.
(239) Stalder, A.; Dürig, U. *Appl. Phys. Lett.* **1996**, *68*, 637.
(240) Stalder, A.; Dürig, U. *J. Vac. Sci. Technol. B* **1995**, *14*, 1259.
(241) Stalder, A.; Durig, U. *Rev. Sci. Instrum.* **1995**, *66*, 3576.
(242) Buttiker, M.; Imry, Y.; Landauer, R.; Pinhas, S. *Phys. Rev. B* **1985**, *31*, 6207.
(243) Scherbakov, A. G.; Bogachek, E. N.; Landman, U. *Phys. Rev. B* **1996**, *53*, 4054.
(244) Olesen, L.; Laegsgaard, E.; Stensgaard, I.; Besenbacher, F.; Schiotz, J.; Stoltze, P.; Jacobsen, K. W.; Norskov, J. K. *Phys. Rev. Lett.* **1994**, *72*, 2251.
(245) Pascual, J. I.; Mendez, J.; Gomez-Herrero, J.; Baro, A. M.; Garcia, N.; Landman, U.; Luedtke, W. D.; Bogachek, E. N.; Cheng, H.-P. *Science* **1995**, *267*, 1793.
(246) Krans, J. M.; Muller, C. J.; Yanson, I. K.; Govaert, T. C. M.; Hesper, R.; van Ruitenbeek, J. M. *Phys. Rev. B* **1993**, *48*, 14721.
(247) Landman, U.; Luedtke, W. D.; Burnham, N. A.; Colton, R. J. *Science* **1990**, *248*, 454.
(248) Lynden-Bell, R. M. *Science* **1994**, *263*, 1704.
(249) Todorov, T. N.; Sutton, A. P. *Phys. Rev. Lett.* **1993**, *70*, 2138.
(250) Pethica, J. B.; Oliver, W. C. *Thin Films: Stresses and Mechanical Properties Symposium*; Bravman, J. C., Nix, W. D., Barnett, D. M., Smith, D. A., Eds.; Mater. Res. Soc: Boston, MA, 1989; p 13.
(251) Landman, U.; Luedtke, W. D.; Salisbury, B. E.; Whetten, R. L. *Phys. Rev. Lett.* **1996**, *77*, 1362.
(252) Butt, H.-J.; Seifert, K.; Bamberg, E. *J. Phys. Chem.* **1993**, *97*, 7316.

(253) Xiao, X.-d.; Liu, G.-y.; Charych, D. H.; Salmeron, M. *Langmuir* **1995**, *11*, 1600.
(254) Nuzzo, R. G.; Allara, D. L. *J. Am. Chem. Soc.* **1983**, *105*, 4481.
(255) Porter, M. D.; Bright, T. B. ; Allara, D. L.; Chidesy, C. E. D. *J. Am. Chem. Soc.* **1987**, *109*, 3559.
(256) Bryant, M. A.; Pemberton, J. E. *J. Am. Chem. Soc.* **1991**, *113*, 8284.
(257) Dubois, L. H.; Zegarski, B. R.; Nuzzo, R. G. *J. Chem. Phys.* **1993**, *98*, 678.
(258) Camillone, N.; Chidsey, C. E. D.; Liu, G.-y.; Scoles, G. *J. Chem. Phys.* **1993**, *98*, 3503.
(259) Fenter, P.; Eisenberg, P.; Liang, K. S. *Phys. Rev. Lett.* **1993**, *70*, 2447.
(260) Fenter, P.; Eberhardt, A.; Eisenberg, P. *Science* **1994**, *226*, 1216.
(261) Yeganeh, M. S.; Dougal, S. M.; Polizzotti, R. S.; Rabinowitz, P. *Phys. Rev. Lett.* **1995**, *74*, 1811.
(262) Wilson, T. E.; Murray, M. N.; Ogletree, D. F.; Bednarski, M. D.; Cantor, C. R.; Salmeron, M. *J. Vac. Sci. Technol. B* **1990**, *9*, 1171.
(263) Wilson, T. E.; Ogletree, D. F.; Salmeron, M.; Bednarski, M. D. *Langmuir* **1992**, *8*, 2588.
(264) Dürig, U.; Züger, O.; Michel, B. *Phys. Rev. B* **1993**, *48*, 1711.
(265) Salmeron, M.; Neubauer, G.; Folch, A.; Tomitori, M.; Ogletree, D. F.; Sautet, P. *Langmuir* **1993**, *9*, 3600.
(266) Poirier, G. E.; Tarlov, M. J. *Langmuir* **1994**, *10*, 2853.
(267) Anselmetti, D.; Baratoff, A.; Güntherodt, H.-J.; Delamarche, E.; Michel, B.; Gerber, C.; Kang, H.; Wolf, H.; Ringsdorf, H. *Europhys. Lett.* **1994**, *27*, 365.
(268) Liu, G.-y.; Fenter, P.; Chidsey, C. E. D.; Ogletree, D. F.; Eisenberger, P.; Salmeron, M. *J. Chem. Phys.* **1994**, *101*, 4301.
(269) Ulman, A. *Introduction to Ultrathin Organic Films from Langmuir-Blodgett to Self-Assembly*; Academic Press: New York, 1991.
(270) Wasserman, S. R.; Tao, Y. T.; Whitesides, G. M. *Langmuir* **1991**, *7*, 532.
(271) Maoz, R.; Sagiv, J. *J. Am. Chem. Soc.* **1984**, *100*, 465.
(272) Wasserman, S. R.; Whitesides, G. M.; Tidswell, I. M.; Ocko, B. M.; Pershan, P. S.; Axe, J. D. *J. Am. Chem. Soc.* **1989**, *111*, 5852.
(273) Tilman, N.; Ulman, A.; Schildkraut, J. S.; Penner, T. L. *J. Am. Chem. Soc.* **1988**, *111*, 6136.
(274) Meyer, E.; Howald, L.; Overney, R.; Brodbeck, D.; Lüthi, R.; Haefke, H.; Frommer, J.; Güntherodt, H.-J. *Ultramicroscopy* **1992**, *42*−44, 274.
(275) Meyer, E.; Overney, R.; Lüthi, R.; Brodbeck, D.; Howald, L.; Frommer, J.; Güntherodt, H.-J.; Wolter, O.; Fujihira, M.; Takano, H.; Gotoh, Y. *Thin Solid Films* **1992**, *220*, 132.
(276) Green, J.-B. D.; McDermott, M. T.; Porter, M. D. *J. Phys. Chem.* **1995**, *99*, 10960.
(277) Overney, R. M.; Meyer, E.; Frommer, J.; Güntherodt, H. J. *Langmuir* **1994**, *10*, 1281.
(278) Overney, R. M.; Leta, D. P. *Tribol. Lett.* **1995**, *1*, 247.
(279) Koleske, D. D.; Barger, W. R.; Lee, G. U.; Colton, R. J. *Thin Solid Films* **1997**, in press.
(280) Xiao, X.-D.; Hu, J.; Charych, D. H.; Salmeron, M. *Langmuir* **1996**, *12*, 235.
(281) Lio, A.; Charych, D.; Salmeron, M. *J. Chem. Phys.*, in press (June, 1997).
(282) Du, Q.; Xiao, X.-d.; Charych, D.; Wolf, F.; Frantz, P.; Ogletree, D. F.; Shen, Y. R.; Salmeron, M. *Phys. Rev. B* **1995**, *51*, 7456.
(283) Guyot-Sionnest, P.; Hunt, J. H.; Shen, Y. R. *Phys. Rev. Lett.* **1988**, *59*, 1597.
(284) Siepman, J. I.; McDonald, I. R. *Phys. Rev. Lett.* **1993**, *70*, 453.
(285) Joyce, S. A.; Thomas, R. C.; Houston, J. E.; Michalske, T. A.; Crooks, R. M. *Phys. Rev. Lett.* **1992**, *68*, 2790.
(286) Salmeron, M. B. *MRS Bull.* **1993**, *18*, 20.
(287) Liu, G.-y.; Salmeron, M. B. *Langmuir* **1994**, *10*, 367.
(288) Lio, A.; Morant, C.; Ogletree, D. F.; Salmeron, M. *J. Phys. Chem.* **1997**, in press (June, 1997).
(289) Salmeron, M.; Liu, G.-y.; Ogletree, D. F. *Forces in Scanning Probe Methods*; Güntherodt, H.-J., Anselmetti, D., Meyer, E., Eds.; Kluwer Academic Publishers: The Netherlands, 1995; p 593.

CR960068Q